Cell

Article

Direct observation of a condensate effect on super-enhancer controlled gene bursting

Graphical abstract

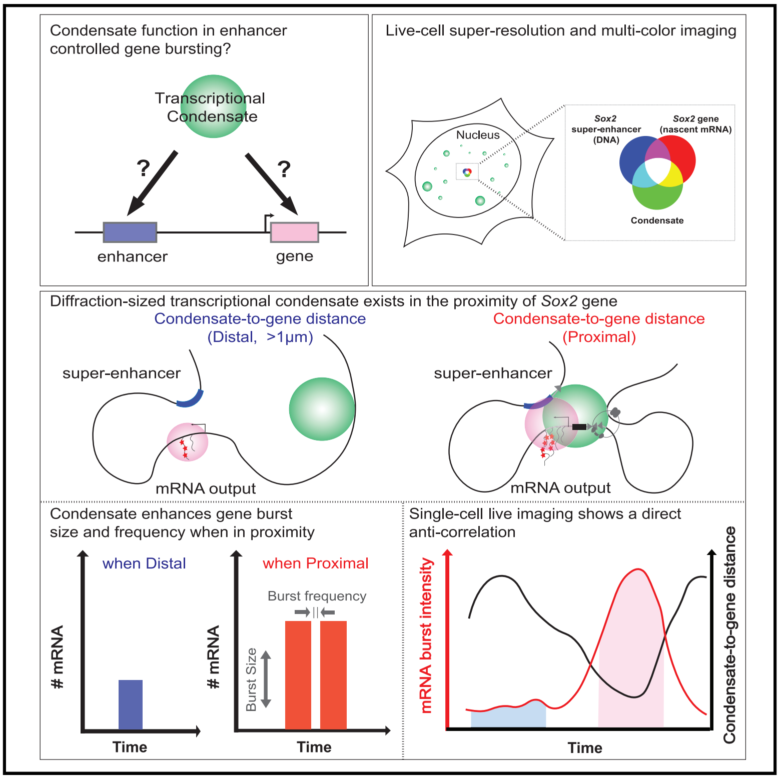

Highlights

- Diffraction-sized transcriptional condensate exists in the proximity of *Sox2* gene
- Condensate enhances gene burst size and frequency when in proximity
- Direct anti-correlation between condensate position and gene burst by live imaging
- Condensate's enhancement depends on local/distal genomic elements and cohesin

Authors

Manyu Du, Simon Hendrik Stitzinger, Jan-Hendrik Spille, ..., Mohammed Hijaz, Andrea Quintana, Ibrahim I. Cissé

Correspondence

cisse@ie-freiburg.mpg.de

In brief

Transcriptional condensate dynamically interacts with the gene locus, resulting in a burst increase when in proximity and a return to basal bursting when the condensate moves away.

Du et al., 2024, Cell *187*, 1–14
January 18, 2024
https://doi.org/10.1016/j.cell.2023.12.005

CellPress

Please cite this article in press as: Du et al., Direct observation of a condensate effect on super-enhancer controlled gene bursting, Cell (2024), https://doi.org/10.1016/j.cell.2023.12.005

Cell

CellPress

Article

Direct observation of a condensate effect on super-enhancer controlled gene bursting

Manyu Du,[1] Simon Hendrik Stitzinger,[1] Jan-Hendrik Spille,[1,2] Won-Ki Cho,[1,3] Choongman Lee,[1] Mohammed Hijaz,[1,4] Andrea Quintana,[1] and Ibrahim I. Cissé[1,5,*]

[1]Department of Biological Physics, Max Planck Institute for Immunobiology and Epigenetics, Freiburg im Breisgau, Baden-Württemberg 79108, Germany

[2]Present address: Department of Physics, University of Illinois, Chicago, IL, USA

[3]Present address: Department of Biological Sciences, KAIST, Daejeon, Republic of Korea

[4]Present address: Department of Biophysics, University of Michigan, Ann Arbor, MI, USA

[5]Lead contact

*Correspondence: cisse@ie-freiburg.mpg.de

https://doi.org/10.1016/j.cell.2023.12.005

SUMMARY

Enhancers are distal DNA elements believed to loop and contact promoters to control gene expression. Recently, we found diffraction-sized transcriptional condensates at genes controlled by clusters of enhancers (super-enhancers). However, a direct function of endogenous condensates in controlling gene expression remains elusive. Here, we develop live-cell super-resolution and multi-color 3D-imaging approaches to investigate putative roles of endogenous condensates in the regulation of super-enhancer controlled gene *Sox2*. In contrast to enhancer distance, we find instead that the condensate's positional dynamics are a better predictor of gene expression. A basal gene bursting occurs when the condensate is far (>1 μm), but burst size and frequency are enhanced when the condensate moves in proximity (<1 μm). Perturbations of cohesin and local DNA elements do not prevent basal bursting but affect the condensate and its burst enhancement. We propose a three-way kissing model whereby the condensate interacts transiently with gene locus and regulatory DNA elements to control gene bursting.

INTRODUCTION

Transcription occurs in episodic processes, characterized by pulsatile bursts.[1–5] Enhancers are *cis*-regulatory elements in the genome that enhance transcription from core promoters in a time- and tissue-specific manner.[6–10] Enhancers are enriched in the higher eukaryotic genomes, and importantly, a significant fraction of enhancers are located at large linear genomic distances from the gene promoters they regulate.[9,11–15] Although the role of enhancers in transcription has been observed in many different cases, their mechanism of action is not fully understood.

We reported on the existence of diffraction-sized condensates of RNA polymerase II (RNA Pol II) and Mediator[16]; however, their function (if any) in gene expression regulation remains unclear. Previously, we and others found that RNA Pol II,[16–21] Mediator, and other cofactors (either endogenously,[16,22] or when imaged in synthetic systems with inserted cassettes of repetitive DNA sites[23,24]) form clusters. In stem cells, around 10% of these clusters are more persistent, and their biophysical properties can be tested[16] and shown to be transcription-dependent condensates. We concluded that this small population of persistent clusters were condensates[25] that are diffraction sized and with liquid-like properties.[16] Our specific interest in this study is that these condensates are found near genes that are controlled by clusters of enhancers, so-called super-enhancers.[16,22] In mouse embryonic stem cells, the pluripotency gene *Sox2* is one of the top super-enhancer controlled genes.[26]

Here, we hypothesize that a condensate may exist near the *Sox2* gene. We developed quantitative live-cell imaging approaches to directly correlate the condensate dynamics to super-enhancer controlled gene bursting. We observe that condensate proximity within an arbitrary threshold distance of 1 μm correlates with enhanced gene bursting and larger variability in the nascent mRNA burst size. The gene burst enhancement depends on proximal weak enhancers and CTCF (CCCTC-binding factor)-binding sites. Genome architectural protein cohesin functions in regulating condensate gene interactions. Upon depletion, the proximity-based burst enhancement is lost, along with an increase in the distance between the condensate and gene locus. Multi-color 3D imaging reveals when the condensate "kisses" the enhancer and the gene locus (three-way kiss), the gene burst size increases; as the condensate moves away, the bursting decreases. Together, our data reveal a role for the spatiotemporal dynamics of transcriptional condensates in regulating gene bursting and have implications on how genome architecture may help to directly control gene expression.

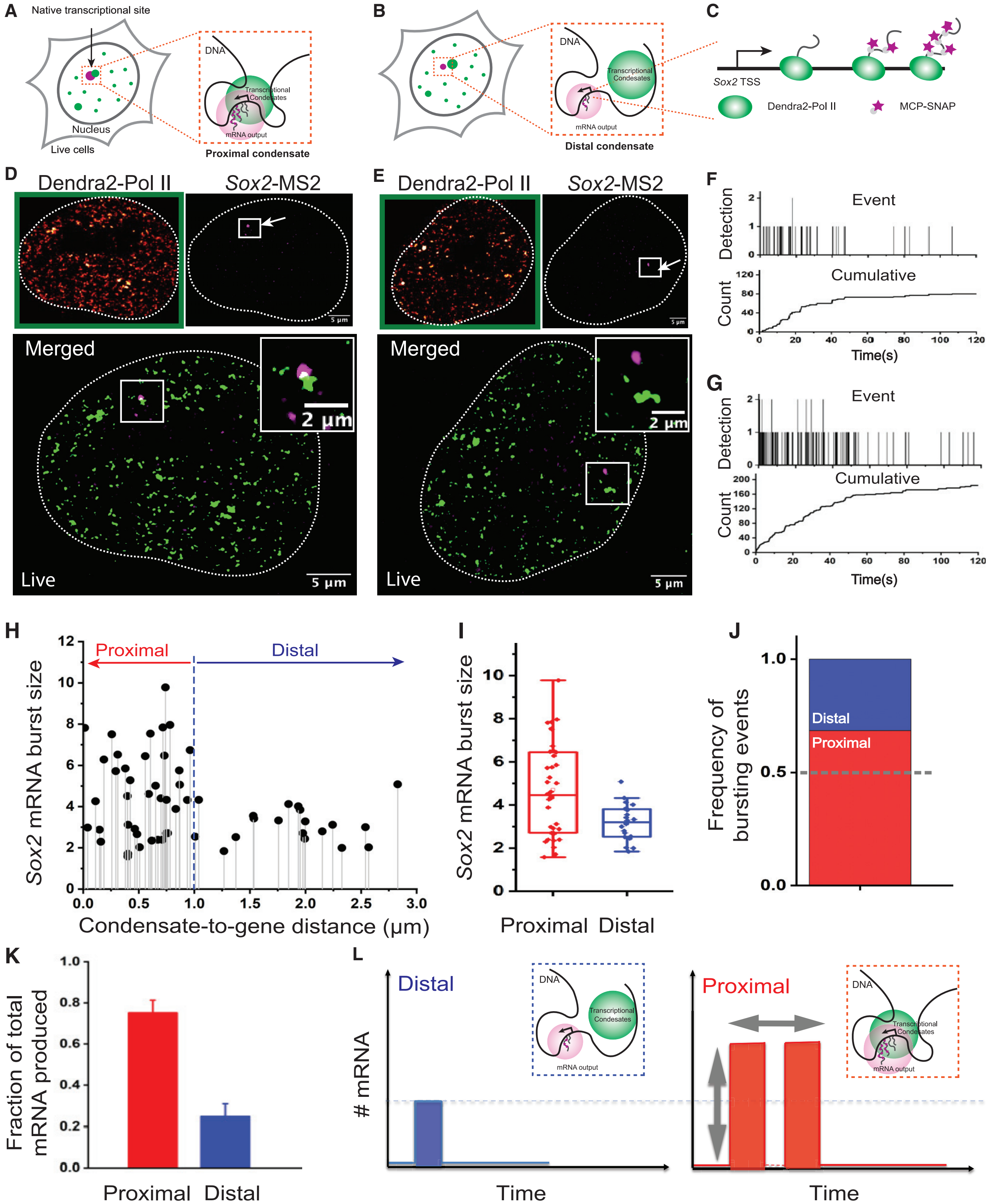

(legend on next page)

RESULTS

Condensate proximity correlates with gene burst enhancement

Condensates manifest as a population of persistent clusters of either RNA Pol II or Mediator in a quantitative live-cell super-resolution imaging approach.[16] Here, we fuse the catalytic subunit of the endogenous RNA Pol II (RPB1, the largest subunit of RNA Pol II) with a green-to-red photoconvertible protein Dendra2, which enables time-correlated photoactivated localization microscopy (tcPALM), the live-cell super-resolution method we developed previously to study the temporal dynamics of sub-diffractive spatial protein clusters.[18] To simultaneously label the endogenous nascent mRNA in the same cells, we engineered 24× MS2 repeats to the 3′ UTR of *Sox2* gene and stably expressed the SNAP-tagged MS2 coat protein (MCP-SNAP) (Figures 1A–1C; STAR Methods). This cell line enables dual-color live-cell and super-resolution imaging of RNA Pol II molecules as well as visualizing the *Sox2* gene locus (Figures 1D and 1E), all while quantifying cluster dynamics by tcPALM and measuring the brightness of *Sox2* mRNA gene burst, which correlates with the number of individual nascent mRNAs synthesized per burst in real time, during gene bursting.[27,28]

We observed a large cell-to-cell variability with the occurrence of a cluster of RNA Pol II on a bursting *Sox2* gene locus: in some cells, RNA Pol II clusters colocalize with *Sox2* active transcription site (Figure 1D), whereas in other cells, we observed the occurrence of a RNA Pol II cluster near *Sox2* transcription site, but not co-localizing with *Sox2* locus (Figure 1E). We imaged and analyzed 76 cells and plotted the estimated number of nascent mRNAs per burst (burst size) as a function of the centroid-to-centroid distance between the gene locus (as evidenced by the localization of the MS2 signal; Figures 1D and 1E) and the nearest persistent/stable RNA Pol II cluster (Figure 1H). We quantified the *Sox2* mRNA burst size as the estimated number of mRNAs by dividing the MS2 intensity at the native transcription site by the mean intensities of single diffusing mRNAs in the cytoplasm (Figures S1A–S1C).

We observed large variability in the burst sizes, and this variability correlates with cluster proximity: beyond an apparent threshold (>1 μm) only a basal burst of 3 ± 0.3 mRNAs is observed, whereas in proximity, burst sizes varied from 1.5 to 10 mRNAs per cell (Figure 1H). We then applied this arbitrary threshold of 1 μm and grouped the data into proximal and distal bursts (Figures 1A and 1B). We observed gene burst sizes of 4.7 ± 0.3 mRNAs per cell when the condensate is in proximity to the gene locus (Figure 1H). On average, *Sox2* mRNA burst size is 1.6-fold higher in the presence of proximal clusters than distal clusters (Figure 1I). Both the proximal and distal RNA Pol II clusters show stable cluster properties,[16] indicated by the cumulative temporal detection traces showing a gradual plateau, and cluster lifetime longer than the total image acquisition time of 2 min (Figures 1F and 1G), similar to the persistent clusters we previously reported.[16]

The bursting dynamics of a gene can be modulated by changes in either burst size or burst frequency. We observed an increase in burst size with proximal clusters (Figures 1H and 1I), and we explored whether cluster proximity also regulates *Sox2* gene bursting frequency. We found that the frequency of bursting events occurring with a proximal cluster is 2-fold higher than that of bursts occurring with a distal cluster (Figure 1J), suggesting higher bursting frequency for proximal clusters.

These results suggest that both the burst size and the bursting frequency are increased with proximity to increase total gene bursting. Consistent with this, when we calculate the integrated mRNA production by proximal vs. distal clusters, we find greater than 75% of the total mRNAs were produced in the presence of a proximal cluster (Figure 1K). Our data suggest that the condensate proximity enhances both burst size and bursting frequency to regulate *Sox2* mRNA production (Figure 1L).

Proximal genomic elements including weak enhancers and CTCF-binding sites are necessary for the condensate's burst enhancement

We were intrigued by the <1 μm threshold and sought to investigate whether there is any possible functional reason for this.

Figure 1. Condensate proximity correlates with an enhancement in *Sox2* gene bursting

(A and B) Schematic showing a condensate proximal (A) or distal (B) to the gene locus.

(C) Zoomed in schematic for mRNA transcripts labeling (magenta) and RNA Pol II (green).

(D) Example of a live-cell, dual color super-resolved image. Two-dimensional super-resolution reconstruction reveals RNA Pol II clusters (upper left) and an actively bursting *Sox2* gene (mRNA labeled by 24× MS2, shown in magenta in upper right). Merged image is shown in (bottom). RNA Pol II clusters are red-hot color coded in the upper left panel and shown as green in the bottom panel. Centroid-to-centroid distance is 0.6 μm in the example shown.

(E) Two-dimensional live-cell super-resolution image of a RNA Pol II cluster (upper left, hot color coded) distal to the active bursting *Sox2* gene (mRNA labeled by 24× MS2, shown in magenta in upper right). Centroid-to-centroid distance is 2.6 μm in the example shown. RNA Pol II cluster is shown in green in the merged images (bottom). Scale bars: 5 μm in (D) and (E) and 2 μm in the insets.

(F and G) tcPALM traces show both proximal (F) and distal (G) RNA Pol II condensates as clusters persisting in time, with a gradual plateau in the cumulative count curves.

(H) Plot of *Sox2* mRNA burst size vs. the distance between the nearest RNA Pol II condensate to the *Sox2* locus.

(I) Boxplots of *Sox2* gene burst size of proximal and distal condensates. N = 76 cells in this analysis. Box edges represent 25–75 percentiles, data outside the whisker represents outliers, and a small open square is used to indicate the mean, whereas the line represents the median. Mean and standard error (SEM) of mRNA burst size is 4.7 ± 0.26 for proximal, and 3 ± 0.31 for distal.

(J) Stack column of the measured frequency of bursting events in proximal and distal cases. Red (proximal) bottom column value is found to be 66% of the bursts, and the blue (distal) top column value 34%. Dashed line is set at 0.5.

(K) Fraction of total mRNA produced by proximal (red bar) and distal condensates (blue bar). Mean and standard error (SEM) is 0.75 ± 0.06 for proximal and 0.25 ± 0.06 for distal.

(L) Schematic summarizing super-resolution data: when condensate is distal a basal gene bursting occurs (left); when the condensate is proximal there is increased gene burst size and increased frequency (right).

See also Figure S1.

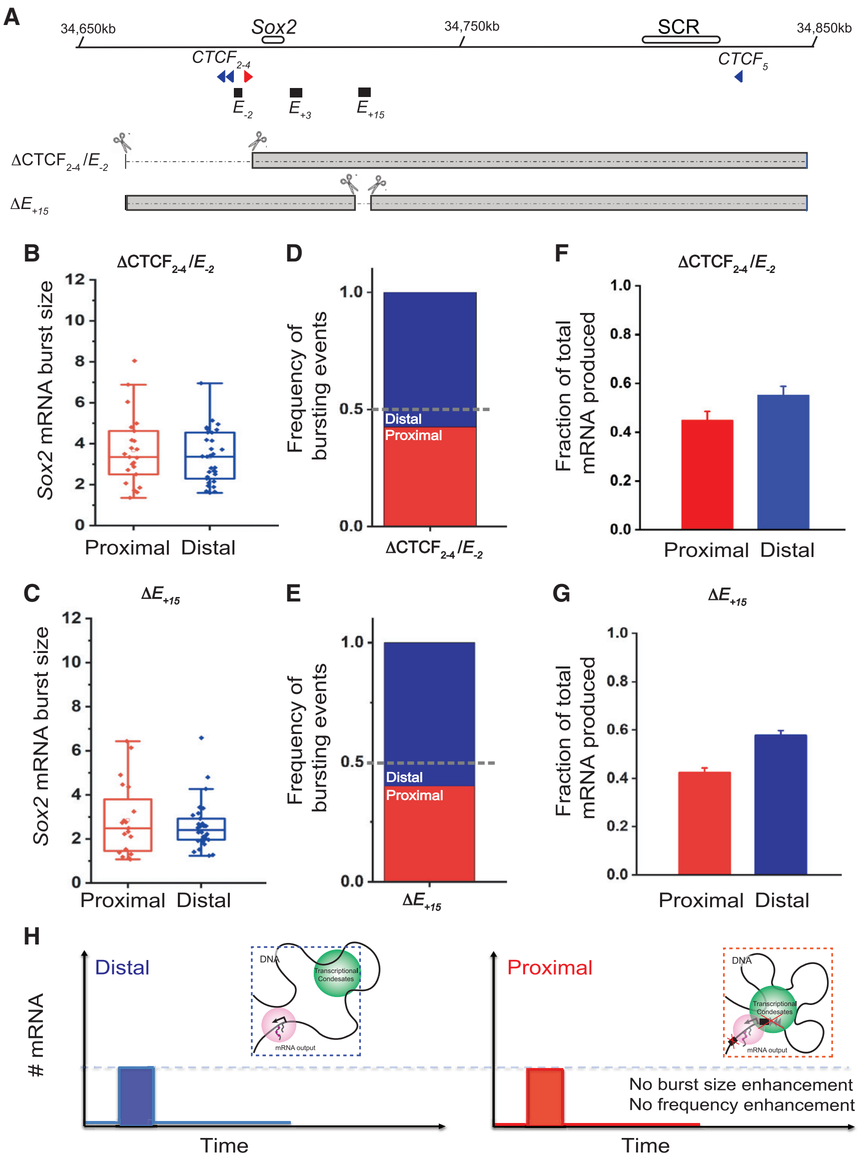

Figure 2. Genomic elements proximal to the gene locus including weak enhancers and CTCF sites are necessary for the condensate's burst enhancement

(A) Schematic of the *Sox2* locus and annotation of CTCF sites and putative weak enhancers. ΔCTCF/E$_{-2}$: deletion of a region containing three CTCF sites upstream and a weak enhancer 2 kb upstream of *Sox2* TSS. ΔE$_{+15}$: deletion of a region containing a weak enhancer 15 kb downstream *Sox2*.

(B) ΔCTCF/E$_{-2}$ deletion abolishes the proximity-based burst enhancement. N = 54 cells were measured by tcPALM. Mean and standard error (SEM) is 3.66 ± 0.35 for proximal and 3.34 ± 0.23 for distal.

(C) ΔE$_{+15}$ deletion abolishes the proximity-based burst enhancement. N = 50 cells were measured by tcPALM. Mean and standard error (SEM) is 2.86 ± 0.36 for proximal, and 2.6 ± 0.2 for distal.

(D and E) Stack column of frequency of bursting events in proximal and distal cases in ΔCTCF/E$_{-2}$ (D) or ΔE$_{+15}$ (E). Dashed line is set at 0.5.

(F and G) Fraction of total mRNA produced by proximal (red bar) and distal condensates (blue bar) in ΔCTCF/E$_{-2}$ (F) or ΔE$_{+15}$ (G) cell lines. Mean and standard error (SEM) is 0.45 ± 0.04 for proximal and 0.55 ± 0.04 for distal in (F). Mean and standard error (SEM) is 0.42 ± 0.02 for proximal and 0.58 ± 0.02 for distal in (G).

(H) Schematic summarizing that deletion of the local genomic elements results in the loss of enhancements in burst size or frequency with condensate proximity (compare to Figure 1L).

See also Figures S2 and S3.

We had previously estimated condensates in general to be diffraction sized (i.e., diameter ∼400–500 nm) in stem cells, but initially wondered whether those associating with *Sox2* might perhaps be larger. We performed structured illumination microscopy (SIM) to measure the diameter of the condensate closest to the *Sox2* locus (Figures S2A–S2D) and confirmed the condensate diameter to be on average 456 ± 201 nm when measured by RNA Pol II or comparably 560 ± 226 nm when measured by Mediator. These results rule out the case that the condensate size alone can account for the 1 μm threshold. We therefore sought to investigate the genomic context proximal to the *Sox2* gene locus.

Sox2 is reported to be regulated by a series of putative enhancer elements within the same topologically associated domain,[29] characterized by DNase I hypersensitivity, histone acetylation, enhancer identification assays (self-transcribing active regulatory region sequencing, referred to as STARR-seq, and luciferase reporters), and genetic perturbations.[29–33] We explored whether putative enhancers are important in regulating the condensate's proximity-based enhancement of *Sox2*. We designed CRISPR gRNAs to delete two proximal DNase I hypersensitive sites (ΔCTCF/E$_{-2}$ and ΔE$_{+15}$), respectively (Figure 2A; STAR Methods), whose deletion in combination with another putative enhancer E$_{+3}$ was shown to reduce *Sox2* gene expression.[30]

Upon each deletion tested, we observed the proximity-based burst enhancement is lost, and there is no difference in *Sox2* gene expression in proximal vs. distal cases (Figures 2B, 2C, and S3). For both the frequency of bursting events (Figures 2D and 2E) and the fraction of total mRNA produced (Figures 2F and 2G), the measured values are comparable (or even slightly less) for proximal vs. distal cases after the enhancer deletion, in contrast to the preferential mRNA production by proximal clusters in the control (normal/wild type) cell line (Figures 1J and 1K). Our data suggest that the CTCF-binding sites and proximal "weak" enhancer regions are important for the condensate's proximal burst enhancement (Figure 2H).

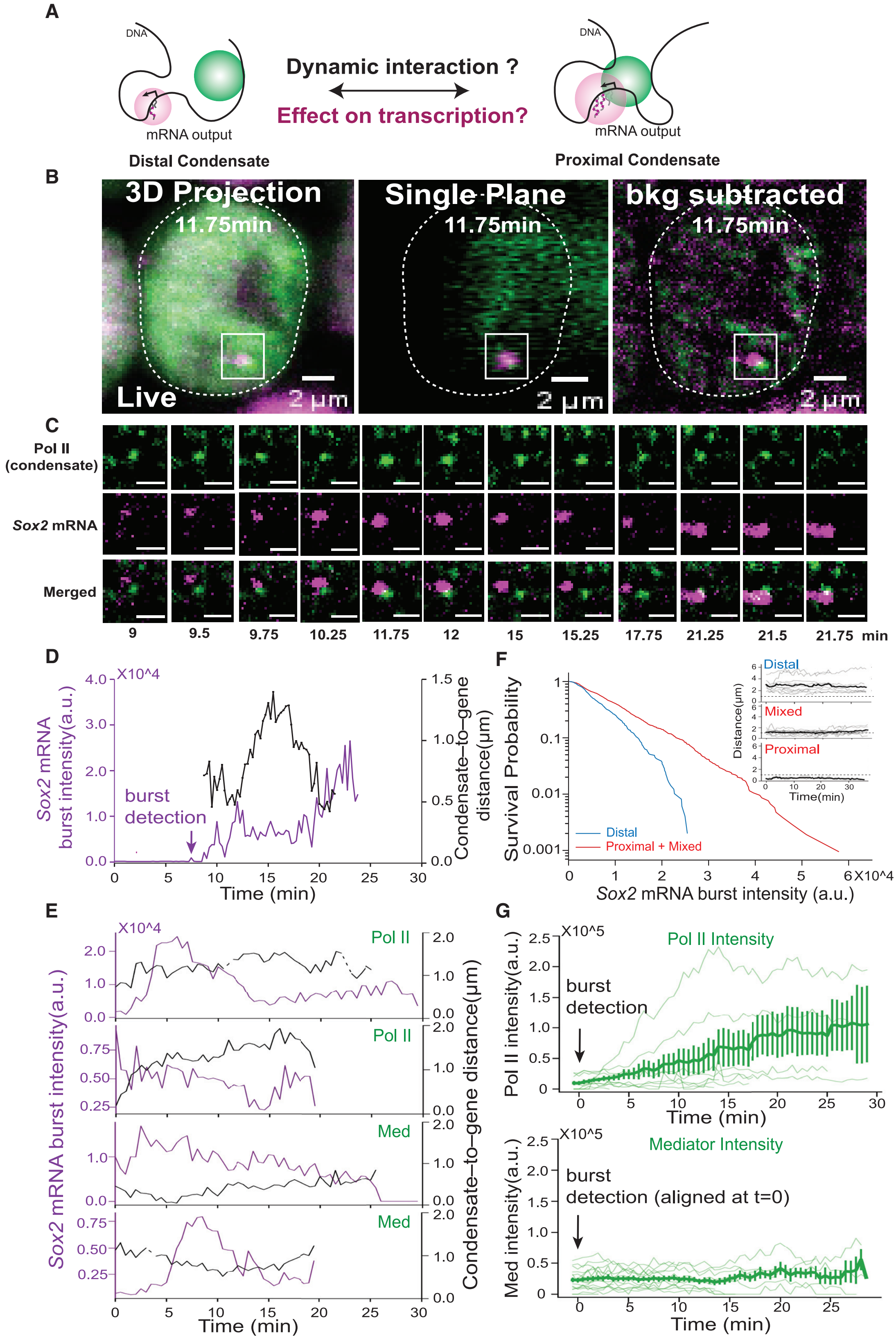

(legend on next page)

Real-time observation of an anti-correlation between gene burst intensity and condensate distance

We next asked whether the proximal and distal clusters represent two distinct cell populations or two dynamic states in the same cell (Figure 3A). We characterized the long-term diffusional dynamics of RNA Pol II condensates and *Sox2* gene locus using lattice light sheet imaging in live stem cells (Video S1). *Sox2* bursts were shown to be short and infrequent, with only 4% of the time spent as a detectable burst using the MS2 system in a previous study.[34] Similarly, we observe *Sox2* bursts in ~20% of cells when imaged longitudinally in time lapse on the lattice light sheet. We observed that RNA Pol II condensates dynamically interact with the *Sox2* gene locus at the single-cell level (Figures 3B and 3C).

There is a direct anti-correlation between burst intensity and the condensate-to-gene distance: *Sox2* nascent mRNA burst intensity is high when the condensate-to-gene distance is low, and burst intensity decreases when the condensate-to-gene distance increases (Figures 3D and 3E). Similar to RNA Pol II as a marker of the condensate, we also observed the same dynamic interactions between Mediator as the marker of the condensate and *Sox2* gene locus at the single-cell level (Figures 3E and S4A–S4C). The distance between the Mediator as a marker of condensate and the gene locus also shows a direct anti-correlation with *Sox2* burst intensity (Figure 3E).

We grouped the imaging traces into "strictly distal" (condensate-to-gene distance stayed above 1 μm throughout the whole imaging time window), "strictly proximal" (condensate-to-gene distance stayed below 1 μm), and "mixed" (condensate-to-gene distance is proximal at some point within the movie). The distal traces show lower *Sox2* burst intensity than the proximal/mixed traces (Figure 3F), corroborating our observation that proximity generally correlates with increased gene bursting (Figures 1H–1L).

In ~25% of the cases, we can observe *de novo* bursting of *Sox2* gene. We therefore align all those traces to time t = 0 when burst starts, and this allows us to ask what happens to the Mediator or RNA Pol II intensities in the condensates after bursting events. We find that the average RNA Pol II intensity increases after the gene burst while Mediator intensity stays unchanged (Figure 3G). This corroborates our previous report[16] that although RNA Pol II and Mediator clusters colocalize in the condensates, upon treating the cells with the transcription inhibitor drug DRB (5,6-dichlorobenzimidazole), RNA Pol II can leave the condensate, whereas Mediator stays, indicating RNA Pol II partitioning into the condensate could be differentially modulated in a transcription-dependent manner. These data suggest to us that upon productive encounter between the condensate and the gene, both entities change: not only does the gene burst increase but the condensate also receives positive feedback to upregulate the partitioning of RNA Pol II into the condensate. In sum, our live cell longitudinal imaging data show a direct real-time anti-correlation between gene burst intensity and condensate-to-gene distance: upon successive kissing events, gene burst intensity increases and as the condensate moves away gene burst intensity decreases. This dynamic process happens at the single-cell level. Moreover, not only does gene burst intensity changes upon condensate kissing but also the condensate composition likely changes with a gradual recruitment of more RNA Pol II.

Three-color live imaging reveals a three-way choreography between SCR, condensate dynamics, and *Sox2* gene bursting in real time

The canonical *Sox2* enhancer is a distal super-enhancer region more than 100 kb from the gene locus, the so-called *Sox2* control region (SCR). The SCR is essential for proper *Sox2* gene expression regulation and stem cell homeostasis.[29–31,33] The textbook model of distal enhancers would predict that the enhancer dynamically loops to contact the gene locus, such that gene burst intensity would be anti-correlated with the enhancer-to-gene distance. However, previous attempts to correlate the enhancer dynamics with gene bursting failed to capture such anti-correlation.[34] Since our approach revealed an anti-correlation between gene burst intensity and condensate-to-gene distance, we sought to capture directly the relative dynamics of all three elements, super-enhancer, bursting gene, and condensate in real time.

To simultaneously resolve the relationship between *Sox2* super-enhancer, transcriptional condensate, and the bursting gene, we performed three-color lattice light sheet imaging to monitor the locations and intensities of SCR, condensate (Mediator or RNA Pol II), and *Sox2* mRNA in real time. We labeled the SCR DNA on Chr 3: 34809948–34816684 (mm9) with a CuO array (144×) that is 5 kb downstream,[34] and the CuO array is

Figure 3. Condensate dynamically interacts with the active *Sox2* gene locus

(A) Schematic of dynamic interactions between the transcriptional condensate and the gene locus.

(B) Live-cell lattice light sheet imaging of condensate and the active *Sox2* gene. Condensate (RNA Pol II) is shown in green, and *Sox2* nascent transcript in magenta. Left panel is an image with 3D maximum intensity projection. Middle panel is the image of the same cell at the same time point (t = 11.75 min) in a single plane. Right panel is the image of 3D projection after background subtraction.

(C) Time course images of the condensate (RNA Pol II) and *Sox2* nascent mRNA cropped from the white square box in (B). Scale bars: 2 μm in (B) and (C).

(D) Plot of *Sox2* mRNA burst intensity (magenta, left y axis) and condensate-to-gene distance (black, right y axis) from data in (C) as a function of time. Arrow indicates where *Sox2* bursting starts to be detected.

(E) Example traces showing anti-correlation between mRNA burst intensity (left y axis, magenta) and condensate-to-gene distance (right y axis, black). Dotted line represents missing frames.

(F) Survival probability of mRNA burst intensities in distal only (blue) vs. proximal/mixed (red) traces. N = 31 bursting traces were analyzed and represented. Survival probability is calculated as 1-probability$_{cumulative}$ and plotted in log linear scale. The distal (top, n = 10), mixed (middle, n = 17), and proximal (bottom, n = 4) traces are plotted as inset. Dashed line in the insets is set at 1 μm.

(G) Plots of RNA Pol II (top) and Mediator (bottom) intensities over the time course after *de novo* bursting. n = 18 traces for RNA Pol II and n = 10 for Med were analyzed. Bursts were plotted to start t = 0. Bold line and error bar represent the average intensity and the standard error of the mean.

See also Video S1 and Figure S3.

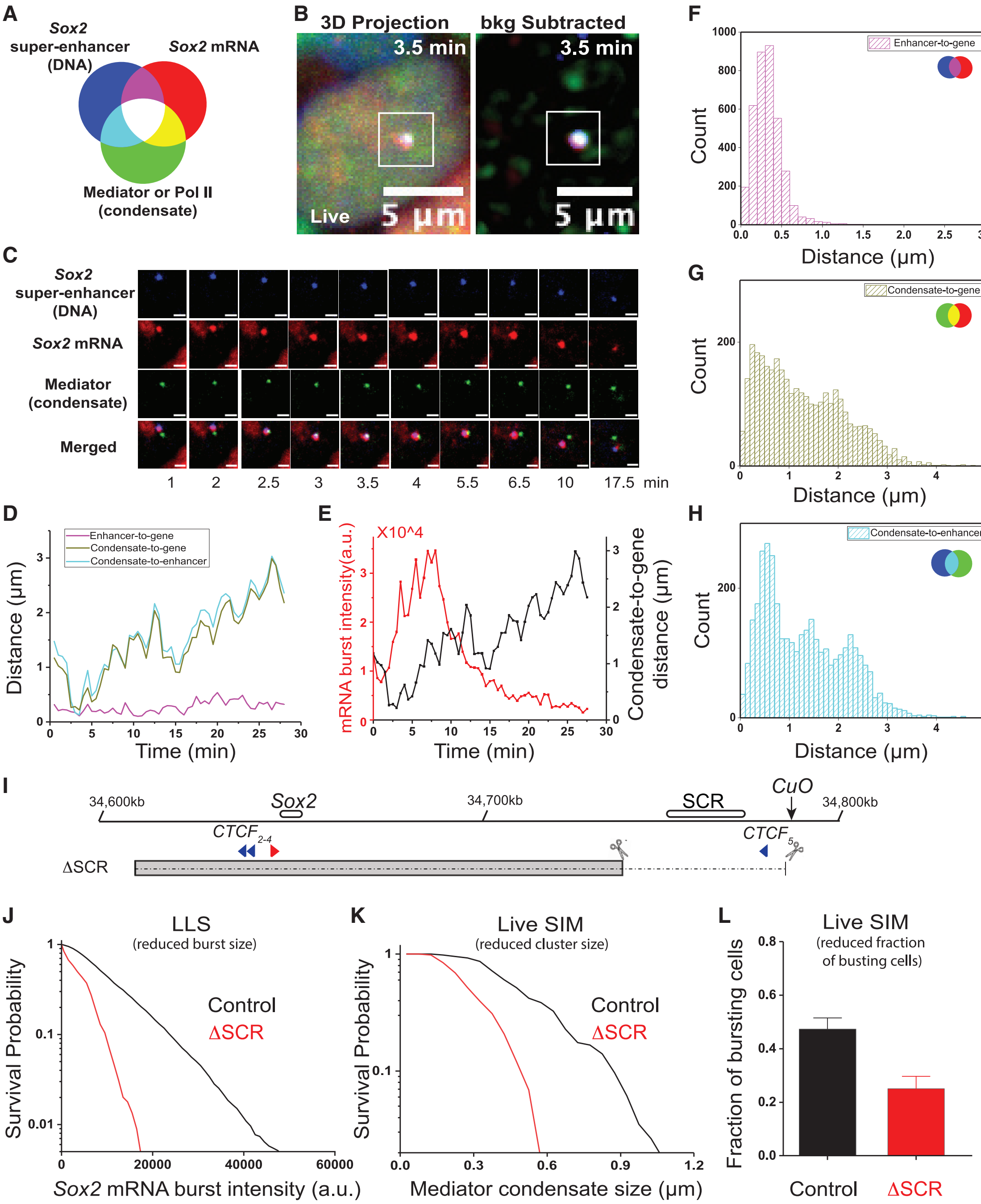

Figure 4. A three-way choreography between *Sox2* super-enhancer (SCR), condensate, and *Sox2* gene bursting in real time

(A) Illustration of a three-color RGB (red, green, blue) scheme. Super-enhancer DNA (SCR) labeled in blue, *Sox2* mRNA labeled by MS2 is in red, and condensate in green.

(B) 3D maximum intensity projection (left) of a cell imaged using live-cell three-color lattice light sheet shows colocalization of *Sox2* super-enhancer (blue), condensate (Mediator, green), and *Sox2* mRNA (red). Scale bars, 5 µm.

(C) Time course images. Scale bars, 2 µm. Images are time courses from the white boxed region in (B).

(D) Plot of distances of enhancer-to-gene (magenta), condensate-to-gene (yellow), and condensate-to-enhancer (cyan) over time from the example in (C).

(E) Plot of *Sox2* mRNA burst intensity (red) and condensate-to-gene distance (black) as a function of time shows a direct anti-correlation.

(F–H) Histograms of centroid-to-centroid distances of enhancer-to-gene (shown in magenta, F), condensate-to-gene (shown in yellow, G), and condensate-to-enhancer (shown in cyan, H). The distances (mean ± standard deviation) are 0.33 ± 0.17, 1.28 ± 0.85, and 1.30 ± 0.83 µm, respectively. Data were collected from time lapse movies taken from N = 58 individual cells.

(legend continued on next page)

fluorescently labeled by *UBCpr*-CymR-EGFP (false-colored blue) and can be marked as a chromatin dot in the nucleus (Figures S2E and S2F; STAR Methods). In the same cell line, we tagged Med19 with Halo (conjugated to Janelia Fluor [JF] dyes colored in green) and *Sox2* mRNA with 24× MS2 repeats labeled by MCP-SNAP (colored in red) as illustrated in Figure 4A.

We analyzed 58 cells showing a gene burst with at least 60% completeness in the track length in all three colors (STAR Methods). Much like in the two-color data in Figure 3, the majority of these unsynchronized cells were in a monotonic state (mostly after a bursting event had already occurred or a bursting event occurring toward the end of the movie).

However, there were several cells where we could capture dynamic changes in the bursting state during the course of our imaging, and as illustrated in the example (Figures 4A–4D and S5A–S5D), these data reveal important qualitative insights. They reveal for instance that the *Sox2* super-enhancer and gene locus can stay at a distance of around 300 nm (indicated by the magenta; Figures 4A–4C and S5A–S5E; Video S2), in line with a previous study that employed this enhancer-labeling strategy.[34] Meanwhile, the condensate pairwise distances (i.e., condensate-to-gene and condensate-to-enhancer) change more significantly in a manner that correlates with gene bursting. The condensates dynamically interact with both the enhancer and gene locus for just a few frames ("three-way kissing" indicated by the white overlapping signal; Figures 4A–4D). Upon a kissing event, here too an anti-correlation between gene burst intensity and the condensate-to-gene distance exists. Upon condensate kissing with gene locus, *Sox2* mRNA burst intensity increases but then dies down when the condensate moves away (Figures 4E and S4D; Video S2).

To more rigorously quantify some of these observations, we pooled the data from all 58 movies and plotted the histograms of centroid-to-centroid pairwise distances. The average distance between the super-enhancer and gene locus is 0.33 ± 0.17 μm (i.e., ~300 nm) (Figure 4F), comparable with what has been reported for SCR and the *Sox2* gene promoter.[34] The average distances for the condensate-to-super-enhancer and condensate-to-gene are 1.30 ± 0.83 and 1.28 ± 0.85 μm, respectively (Figures 4G and 4H). Similar observations are made when using RNA Pol II as the marker for condensates or using Mediator as the label (Figures S5A–S5E; Video S3). RNA Pol II condensates also dynamically interact with both the enhancer and gene locus (Figures S5A–S5E; Video S3).

Furthermore, with the pooled data, we plotted the *Sox2* mRNA burst intensity as a function of condensate-to-gene distance for each frame in the three-color labeled cell line, a proxy for measuring of burst intensity as a function of condensate-to-gene distance analogous to what we did for the super-resolution data but with the data from all cells from lattice light sheet instead of the few hand-picked individual examples represented in the Figures 4A–4D. Here as well, we observed the *Sox2* burst intensities are significantly higher with proximal condensates compared with distal condensates (Figure S5F) corroborating our live cell super-resolution conclusions in Figure 1. Using the same arbitrary threshold of 1 μm used in the super-resolution analysis, the average proximal burst intensity is 2.7-fold higher than distal burst intensity (Figure S5G). Overall, the lattice-light sheet data corroborate our live-cell super-resolution observations in Figure 1 and reveal in addition that the condensate dynamically overlaps with the enhancer and gene locus with a real-time anti-correlation between gene bursting and the condensate's distance.

Condensate does not remain associated with the super-enhancer (SCR), but the SCR deletion negatively affects condensate size and gene bursting

Implicit in the three-color data is the surprise (to us) that the condensate does not remain statically associated with the super-enhancer (SCR). This is contrary to our prior assumptions that condensates likely formed and remained at super-enhancer. Thus, we aimed to test whether deletion of the SCR had any effect on the condensate and the observed gene burst enhancements. We performed a deletion of the SCR similar to that performed in a previous study[30] to investigate the effects on our current observations. Briefly, we designed CRISPR gRNAs to delete a 33 kb region including the ~14 kb SCR and its neighboring region, which also contains the CTCF site at the topologically associating domain (TAD) boundary of *Sox2* (Figure 4I) in both dual-color cell line and the three-color cell line. All the cell lines we got have heterozygous SCR deletion, possibly due to the lethality of homozygous deletion in 2i stem cell growth condition. Therefore, we proceed with the caveat that with a heterozygous SCR deletion. We cannot rule out that any observed remaining effect could be due to possible compensation of the surviving *Sox2* allele.

Nonetheless, these cells could allow us to conclude that the SCR was essential for all our observations on the condensate and gene bursting. Using the lattice light sheet imaging, we find that the *Sox2* mRNA burst intensity decreases after SCR deletion (Figure 4J). In addition, we observed a decrease in the fraction of total bursting cells by 50% (Figure 4L). By using SIM to measure the condensate size in live cells, we find the median diameter of Mediator cluster proximal to *Sox2* gene falls from 516 ± 226 nm normally to 316 ± 136 nm upon SCR deletion, suggesting a reduction in the *Sox2*-associating condensate from

(I) Schematic presentation of the *Sox2* locus in mESCs. The CuO array was inserted 5 kb downstream the *Sox2* super-enhancer (SCR). ΔSCR: deletion of a 33 kb region while preserving the inserted CuO array.

(J) Survival probability plot of mRNA burst intensities in the control cell line (black curve) and ΔSCR cell line (red curve). N = 58 traces for control and N = 10 bursting traces for ΔSCR.

(K) Survival probability plot of Mediator condensate size (Feret's diameter) in control (black curve) and ΔSCR (red curve). Median ± standard deviation is 516 ± 226 nm for the control (black) and 316 ± 136 nm for the ΔSCR (red) *cell* line. N = 114 cells for control and N = 58 cells for ΔSCR imaged using live-cell SIM.

(L) Fraction of bursting cells in the control (black) and ΔSCR (red) cell lines. Data in (K) and (L) were collected using live structured illumination microscopy. Mean and standard error (SEM) is 0.47 ± 0.02 for the control cell line and 0.25 ± 0.04 for SCR deletion cell line.

See also Video S2 and Figure S4.

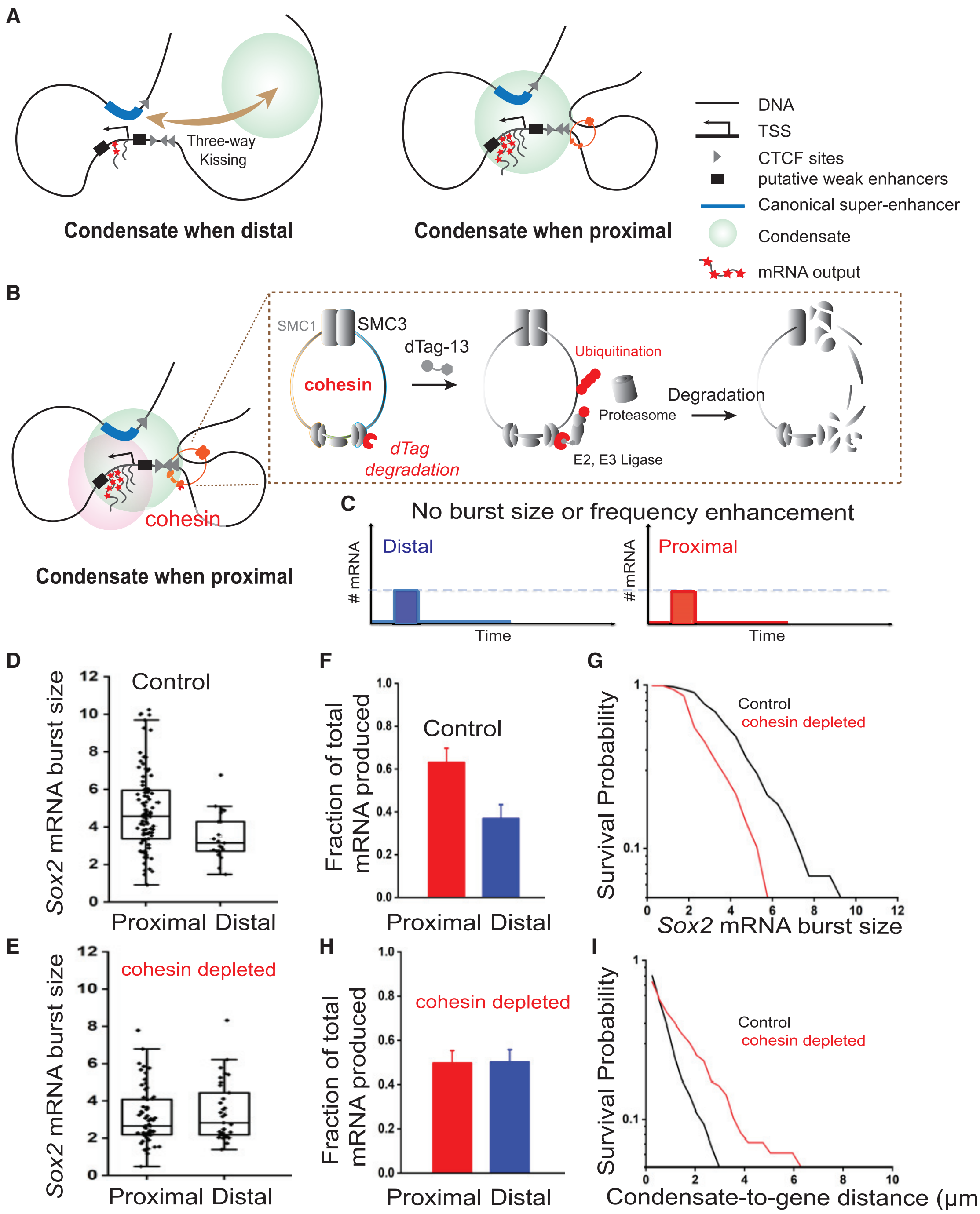

Figure 5. Productive condensate-gene locus kissing is likely dependent on cohesin activity

(A) A three-way kissing model of gene burst enhancement by transcriptional condensates. When the condensate is distal, there is basal gene bursting; when the condensate kisses the super-enhancer, the gene with proximal *cis*-regulatory elements, there is a burst enhancement.

(B) Schematic of rapid cohesin degradation using the dTAG system.

(C) Schematic predicting bursting dynamics with no enhancement in burst size or frequency with proximal condensates after cohesin depletion.

(D) Boxplots of *Sox2* burst sizes in the presence of proximal RNA Pol II condensates (n = 73 cells) and distal condensates (n = 45 cells). Data were collected under the control condition without cohesin depletion. Mean and standard error (SEM) of mRNA burst size is 4.87 ± 0.2 for proximal, and 3.49 ± 0.27 for distal.

(E) Boxplots of *Sox2* burst sizes in the presence of proximal RNA Pol II condensates (n = 52 cells) and distal condensates (n = 46 cells) with cohesin depletion. Mean and standard error (SEM) of mRNA burst size is 3.16 ± 0.21 for proximal, and 3.28 ± 0.23 for distal.

(legend continued on next page)

Please cite this article in press as: Du et al., Direct observation of a condensate effect on super-enhancer controlled gene bursting, Cell (2024), https://doi.org/10.1016/j.cell.2023.12.005

large persistent cluster to a size nearly undetectable by conventional imaging (Figure 4K). Our data suggest that although the condensate does not remain statically associated with the SCR, the SCR is nonetheless critical for the large condensate sizes and the enhanced gene bursting we observed.

Productive condensate-gene locus kissing is likely dependent on cohesin activity

One possibility is that the mere passive proximity of condensate could result in the sudden enhancement of gene bursting. Another possibility is that when in proximity, an active process, perhaps too transient for us to capture, may be needed to effect gene burst enhancement. Integrating our various observations led us to further explore a possible missing link in how the condensates induce burst enhancement when in proximity.

In a previous study,[17] we found that the dwell time (i.e., the lifetime directly on the gene locus) of transient clusters of RNA Pol II that assemble on the β-actin gene locus (and disassemble a few seconds later) correlated linearly with the number of mRNAs subsequently produced: every 2 s the cluster stayed co-localized on the β-actin gene locus corresponded to an increase of an additional mRNA per burst, such that in 8 s, those clusters could produce 4 messenger RNAs the basal β-actin burst size.[17] If a similar process could be at play in our current *Sox2* data, then the enhanced burst size observed in Figure 1H could be accounted for by a transient event that holds the cluster to directly colocalize for 10–12 s. Since the condensate manifests as stable/persistent RNA Pol II clusters, tcPALM alone would not discriminate the exact colocalization time in our current study. The lattice light sheet imaging sampled at a rate of 15–30 s per frame to allow long-term (∼30 min) longitudinal movies may also miss a functional kissing event of less than 15 s. Therefore, we could be blind to transient, productive kissing events.

Interestingly, several differences exist between the previous study and the current study: notably, no persistent clusters (only transient clusters) were present for β-actin, and no frequency enhancement (only burst size enhancement) occurred with β-actin. Also notable here is that the genomic elements proximal to the *Sox2* gene locus (putative weak enhancers and clusters of CTCF-binding sites) are important for gene burst enhancement. Without a proximal condensate, the gene locus (even with a looped SCR at 300 nm) seems to drive only a basal gene bursting (no burst size nor frequency enhancement) (Figure 5A). These results pointed us to look for genome architectural proteins as a possible hidden contributor.

Moreover, from the two- and three-color time-lapse movies, it appears that only when the condensate moves in proximity and seemingly kisses the gene locus that the nascent mRNA signal increases suggesting burst enhancement, and when the condensate moves away, the mRNA signal decreases (Figure 5A). We wondered whether the genome architectural protein cohesin—which can dynamically mediate long-range DNA looping—could be an important missing factor.

We fused SMC3 (structural maintainance of chromosome protein 3), a structural subunit of the cohesin complex, with a degrader FKBP12^{F36V} to study the effect of cohesin degradation using the dTAG system (Figure 5B). The efficiency of degradation is evaluated by western blot, and 1-h treatment of dTAG13 at 500 nM is sufficient to deplete SMC3 in the cells (Figure S3F). The control condition of this new cell line but without treatment with dTAG13 was in good agreement with Figure 1I, as we observed that the average *Sox2* burst size with proximal clusters is 4.9 ± 0.2 mRNAs per burst, and the distal ones 3.5 ± 0.3 mRNAs per burst (Figure 5D).

After acute depletion of SMC3, notably, we still observed gene bursting as well as the presence of condensates. However, there is no gene burst enhancement of *Sox2* by condensate proximity (Figures 5E, S3H, and S3J), although the gene can still produce a basal burst. For both *Sox2* bursting that are proximal (<1 μm) and distal (>1 μm) to the condensate, there is no significant difference in bursting intensity and both at the basal level, with a burst size of 3.2 ± 0.2 and 3.3 ± 0.2, respectively. The fraction of total mRNA produced by proximal and distal cases becomes comparable after cohesin deletion (Figure 5H), in contrast to the preferential mRNA production by proximal clusters in the control condition without depletion (Figure 5F).

We analyzed the distributions of *Sox2* mRNA burst sizes represented by the survival probabilities with and without SMC3 depletion, and we found that cohesin depletion leads to a decrease in mRNA burst sizes (Figure 5G). Accordingly, the distances between the condensate and *Sox2* gene locus increase after SMC3 depletion (Figure 5I). Our data suggest that although the condensate can diffuse in proximity to the gene locus, cohesin is required for the condensate's ability to enhance *Sox2* gene bursting, including both burst size and burst frequency.

Thus, the mere "proximity" of the condensate to the gene locus is not alone driving gene burst enhancement. We propose instead that cohesin, through its proposed looping extrusion, may help bring and hold the condensate to colocalize transiently on the gene with a sufficient dwell time to drive the observed increases in gene bursting (for a purely qualitative illustration of this proposed model, see cartoon depiction in Video S4).

DISCUSSION

In this study, we investigate the function and dynamics of transcriptional condensates in the context of super-enhancer controlled gene *Sox2*. *Sox2* has a very short gene length of 2.4

(F) Fraction of total mRNA produced by proximal (red bar) and distal condensates (blue bar) in the control condition without cohesin depletion. Mean and standard error (SEM) is 0.63 ± 0.07 for proximal and 0.37 ± 0.07 for distal.

(G) Survival probability plots of all MS2 burst sizes under control (shown in black) and cohesin depleted (shown in red) condition.

(H) Fraction of total mRNA produced by proximal (red bar) and distal (blue bar) with cohesin depletion. Mean and standard error (SEM) is 0.5 ± 0.06 for proximal and 0.5 ± 0.06 for distal.

(I) Survival probability plots of condensate-to-gene distances under control (shown in black) and cohesin depleted (shown in red) condition. Data were plotted in log linear scale.

See also Figure S3.

kb; hence, we hypothesized that if there is a direct function of transcriptional condensates on *Sox2* gene bursting, we should be able to resolve the correlation within the timescales of our live imaging capabilities. Indeed, we observed a direct anti-correlation between the gene burst intensity and the distance between condensate-to-gene locus (Figures 3D and 3E).

The classic, textbook model suggests that an enhancer and gene promoter form physical one-to-one interaction through long-range DNA looping. Evidence for such long-range interactions exists by contact-mapping sequencing techniques like HiC (high-throughput chromosome conformation capture), ORCA (optical reconstruction of chromatin architecture), 3D FISH, etc.[35–39] However, recent imaging data challenge the notion of an anti-correlation between enhancer-promoter distance and gene expression. For example, in *Drosophila*, a single enhancer can simultaneously co-regulate the bursting of two genes,[40] thus contradicting the one-to-one interaction model. Anti-correlation of enhancer-promoter distance to gene bursting was observed in labeled *eve* enhancer and an inserted, exogenous PP7 reporter gene,[41] but the enhancer-promoter distance gap when the reporter gene is ON remained larger than 300 nm. In mammalian cells, the distance between the sonic hedgehog (*Ssh*) gene and its enhancer increases up to 1 μm upon gene activation during neuronal differentiation, in contrast to expectation of increased proximity.[42] In fact, for *Sox2*, live imaging of the enhancer and promoter DNA elements showed no difference in enhancer-promoter distance in bursting and non-bursting cells.[34] These results put in question our fundamental understanding of how distal *cis*-regulatory elements work to dynamically control gene bursting in real time in living cells.

We find here that there is a persistent condensate of RNA Pol II and Mediator in the proximity of the *Sox2* gene. The size of the transcriptional condensate near *Sox2* gene, which we measure to have an average Feret's diameter of 456 ± 201 nm (for RNA Pol II) and 560 ± 226 nm (for Mediator), is perfectly appropriate to bridge a gap of ~300 nm, if it exists,[43] between super-enhancer and gene locus (Figures S2A–S2D). Our results reveal that the condensate is an important factor missing in prior studies and a better predictor of gene bursting than enhancer DNA distance.

Genome architectural proteins such as cohesin are proposed to act by loop extrusion to create TADs.[44–46] These TAD structures provide a mechanism to regulate transcription by increasing probabilities of enhancer-gene promoter contacts within a TAD and decreasing probabilities of enhancer-promoter contacts between TADs. However, recent genome-wide studies investigating the depletion of cohesin or cohesin-regulating proteins challenge these assumptions at the transcriptionally important level of enhancer and gene locus interactions,[47–49] including specifically around the *Sox2* locus.[29,30,50]

In this context too, our results provide new insights. We find that cohesin depletion does not affect basal *Sox2* gene bursting but instead prevents the condensate's gene burst enhancement (Figures 5D and 5E). Our data show that rapid depletion of cohesin leads to an increase in condensate-to-gene distance (Figure 5I) and a reduction in burst size (Figure 5G). Further dissection of the data shows that these changes in gene bursting result from a loss in the condensate's ability to enhance gene burst compared with basal bursting (compare Figure 5E with Figure 5D); and there is no burst frequency changes when condensate is in proximity (compare Figure 5H with Figure 5F). These results suggest a likely function for cohesin in mediating the kissing interaction between condensate and gene locus.

It was surprising to us that condensate does not remain stably associated with the canonical super-enhancer (SCR) as we previously assumed.[22] Previous studies[51,52] on nuclear speckles effects on gene expression motivated us to also investigate whether the transcriptional condensates are identical to speckle sites. However, our data rule out that possibility; the transcriptional condensates are distinct from speckles (Figure S1D). Thus, we do not know where the condensate is located.

We favor a model where the condensate remains associated with chromatin (Figure 5A), perhaps in other *cis*-regulatory regions, and perhaps even further away than SCR (given how compact the locus is in chromatin tracing data[39] compared with our observed distances). Such a model would account for all our previous observations of the condensates diffusing at the same rate as other chromatin domains, and results of drug treatments, like JQ1 (a BET bromodomain inhibitor),[53] which prevent association of BET bromodomains to chromatin and result in the disappearance of all RNA Pol II and Mediator clusters, including persistent condensates.[16] This model can also explain more readily the effect of cohesin in regulating a functional association of the condensate with both the gene locus and canonical enhancer. We speculate that the canonical super-enhancer (SCR) is still essential in forming and maintaining the condensate even if the condensate does not remain associated; this idea is supported by our observation that SCR deletion has marked effects on both condensate size (Figure 4K), the burst intensity (Figure 4J), and the fraction of bursting cells (Figure 4L). However, further investigation is needed to study where the condensate initiates or resides. Nonetheless, our study reveals the spatiotemporal dynamics of condensates as a critical factor in our understanding of gene expression regulation by distal enhancers.

Limitations of the study

In the proposed kissing model, a kissing event refers to an encounter between the condensate and the gene locus. We suspect that productive encounters have rather transient dwell times—likely on the order ~12 s based on estimates from our previously published work on the dwell time of colocalization of transient RNA Pol II clusters on a gene locus and its linear correlation with gene burst output[17]—before the condensate diffuses away. This could explain why both the super-resolution and the time-lapse light sheet imaging (15–30 s time intervals) tend to capture proximity rather than perfect overlap.

Another limitation is that we have not directly labeled the promoter in this study and use the MS2 (nascent mRNA signal) as a proxy for the locus of the bursting gene. This is in part because strategically we chose to have the enhancer DNA and the condensate labeled in the three-color dynamic colocalization. Another reason is that our measurement is in good agreement with a previous study[34] showing that there is no measurable difference between using a promoter label (8 kb upstream of the promoter) or using the MS2 signal as the indicator for the *Sox2* gene locus. Therefore, labeling the promoter should not change the conclusions of this study.

This design allows us to address the bursting gene locus, but not the periods when the gene is off. For instance, we can point out that in nearly all cases where we detected a bursting gene, there is condensate in the vicinity: 75%–80% of all *Sox2* mRNAs were produced with a condensate within <1 μm of the bursting gene and the remaining 20%–25% of mRNAs were produced, still, with a condensate that has moved to a distance >1 μm, suggesting that the condensate may have already played a role in facilitating the gene activity. Thus, without synchronizing *Sox2*-bursting events, and without labeling the promoter, we stopped short of concluding that almost every bursting event likely started with a condensate.

The cartoon illustrations (Video S4) make assumptions about where the condensate is located, which, as discussed above, is unknown. It also makes assumptions about cohesin, which is based on others' findings. For instance, it is unclear in the literature where exactly cohesin loads on chromatin. However, the loader of cohesin (called NIPBL, nipped-B-like protein) is shown to interact with Mediator[54,55]; hence, it is tempting to propose that cohesin could load at the condensate, given that there is a cluster of Mediator, but this is pure speculation. Then, cohesin is also proposed to bring distal genomic regions through a dynamic process called loop extrusion[56,57] with CTCF acting as a barrier,[58] but we have no direct evidence for this in this study except that deleting CTCF-binding sites or depleting cohesin would both affect the condensate's ability to enhance gene bursting. Nonetheless, the qualitative aspects of the model are independent of these assumptions on where exactly cohesin is loaded and how cohesin mediates looping *in vivo*. Further investigations into chromatin architecture could falsify these assumptions in future studies.

Future outlooks

It had been difficult to determine a direct, functional association between transcriptional condensates and gene activity endogenously. Here, the observations for *Sox2* help us understand how distal enhancers can dynamically regulate gene expression in real time. A similar approach may be used to study condensate functions in other contexts.

Finally, in the field, it is sometimes assumed that varying enhancers work identically in their mechanisms of regulation of gene expression. In addition to the *Sox2* gene locus, the quantitative imaging and analysis approaches developed here may help in the future to discern key differences in the mechanisms of action between different enhancer condensates and gene loci.

STAR★METHODS

Detailed methods are provided in the online version of this paper and include the following:

- KEY RESOURCES TABLE
- RESOURCE AVAILABILITY
  - Lead contact
  - Materials availability
  - Data and code availability
- EXPERIMENTAL MODEL AND SUBJECT DETAILS
- METHOD DETAILS
  - Mouse embryonic stem cell (mESC) culture
  - mESC cell line engineering
- QUANTIFICATION AND STATISTICAL ANALYSIS
  - tcPALM analysis
  - Quantification of burst size, burst frequency, total fraction of mRNA
  - Condensate size measurement
  - Lattice light sheet imaging analysis

SUPPLEMENTAL INFORMATION

Supplemental information can be found online at https://doi.org/10.1016/j.cell.2023.12.005.

ACKNOWLEDGMENTS

We thank members of the Cissé Department for critical input and past members of the lab at MIT & Caltech (especially J.O. Andrews, F. Pir-Cakmak, M. Zheng, R. Amin, and Z. Ye). We thank L.D. Lavis (HHMI, Janelia) for gift of JF dyes. We thank Dr. J.O. Andrews and Zitian Ye for assistance with the tcPALM analysis software. We thank B. Ren (and members of Ren group, UCSD), A. Boettiger (Stanford), E. Nora (UCSF), L. Georgetti (FMI Basel), and P. Rocha (NICHD/NIH) for helpful discussion about genome architecture and J. Marko (Northwestern U.) and R. Young (MIT) for helpful discussion about Cohesin recruitment. We thank anonymous reviewers for suggestions that impacted the paper. We also thank the imaging and FACS facilities at MPI-IE Freiburg for their support. This work was supported by core funding from the Max Planck Society to I.I.C. and by NIH grant 5R01GM134734 to I.I.C. I.I.C. is PEW Scholar and Macarthur Fellow, which provided support. I.I.C. is scientific member and director in the Max Planck Society, which supports all the research in the Department of Biological Physics at MPI-IE Freiburg.

AUTHOR CONTRIBUTIONS

M.D. and I.I.C. conceived of and designed the study. M.D. and S.H.S. performed the microscopy experiments and data analysis. S.H.S. and M.H. helped with the lattice light sheet data analysis. C.L. and A.Q. helped with stem cell culture. M.D., C.L., W.-K.C., and J.-H.S. contributed to cell line generation. M.D. and I.I.C. wrote the manuscript with input from all coauthors. I.I.C. supervised all aspects of the project.

DECLARATION OF INTERESTS

I.I.C. is on the Advisory Board at *Cell*.

Received: May 9, 2023
Revised: October 29, 2023
Accepted: December 4, 2023
Published: January 8, 2024

REFERENCES

1. Chong, S., Chen, C., Ge, H., and Xie, X.S. (2014). Mechanism of transcriptional bursting in bacteria. Cell *158*, 314–326.
2. Corrigan, A.M., Tunnacliffe, E., Cannon, D., and Chubb, J.R. (2016). A continuum model of transcriptional bursting. eLife *5*, e13051.
3. Coulon, A., Chow, C.C., Singer, R.H., and Larson, D.R. (2013). Eukaryotic transcriptional dynamics: from single molecules to cell populations. Nat. Rev. Genet. *14*, 572–584.
4. Miller, O.L., and McKnight, S.L. (1979). Post-replicative nonribosomal transcription units in *D. melanogaster* embryos. Cell *17*, 551–563.
5. Sanchez, A., and Golding, I. (2013). Genetic determinants and cellular constraints in noisy gene expression. Science *342*, 1188–1193.

6. Banerji, J., Rusconi, S., and Schaffner, W. (1981). Expression of a beta-globin gene is enhanced by remote SV40 DNA sequences. Cell *27*, 299–308.

7. Bulger, M., and Groudine, M. (2011). Functional and mechanistic diversity of distal transcription enhancers. Cell *144*, 327–339.

8. Maston, G.A., Evans, S.K., and Green, M.R. (2006). Transcriptional regulatory elements in the human genome. Annu. Rev. Genomics Hum. Genet. *7*, 29–59.

9. Shen, Y., Yue, F., McCleary, D.F., Ye, Z., Edsall, L., Kuan, S., Wagner, U., Dixon, J., Lee, L., Lobanenkov, V.V., et al. (2012). A map of the cis-regulatory sequences in the mouse genome. Nature *488*, 116–120.

10. Spitz, F., and Furlong, E.E. (2012). Transcription factors: from enhancer binding to developmental control. Nat. Rev. Genet. *13*, 613–626.

11. Carey, M. (1998). The enhanceosome and transcriptional synergy. Cell *92*, 5–8.

12. ENCODE Project Consortium (2012). An integrated encyclopedia of DNA elements in the human genome. Nature *489*, 57–74.

13. Levine, M., and Tjian, R. (2003). Transcription regulation and animal diversity. Nature *424*, 147–151.

14. Pombo, A., and Dillon, N. (2015). Three-dimensional genome architecture: players and mechanisms. Nat. Rev. Mol. Cell Biol. *16*, 245–257.

15. Visel, A., Rubin, E.M., and Pennacchio, L.A. (2009). Genomic views of distant-acting enhancers. Nature *461*, 199–205.

16. Cho, W.K., Spille, J.H., Hecht, M., Lee, C., Li, C., Grube, V., and Cisse, I.I. (2018). Mediator and RNA polymerase II clusters associate in transcription-dependent condensates. Science *361*, 412–415.

17. Cho, W.K., Jayanth, N., English, B.P., Inoue, T., Andrews, J.O., Conway, W., Grimm, J.B., Spille, J.H., Lavis, L.D., Lionnet, T., et al. (2016). RNA polymerase II cluster dynamics predict mRNA output in living cells. eLife *5*, e13617.

18. Cisse, I.I., Izeddin, I., Causse, S.Z., Boudarene, L., Senecal, A., Muresan, L., Dugast-Darzacq, C., Hajj, B., Dahan, M., and Darzacq, X. (2013). Real-time dynamics of RNA polymerase II clustering in live human cells. Science *341*, 664–667.

19. Iborra, F.J., Pombo, A., Jackson, D.A., and Cook, P.R. (1996). Active RNA polymerases are localized within discrete transcription "factories' in human nuclei. J. Cell Sci. *109*, 1427–1436.

20. Li, J., Dong, A., Saydaminova, K., Chang, H., Wang, G., Ochiai, H., Yamamoto, T., and Pertsinidis, A. (2019). Single-molecule nanoscopy elucidates RNA polymerase II transcription at single genes in live cells. Cell *178*, 491–506.e28.

21. Wang, H., Li, B., Zuo, L., Wang, B., Yan, Y., Tian, K., Zhou, R., Wang, C., Chen, X., Jiang, Y., et al. (2022). The transcriptional coactivator RUVBL2 regulates Pol II clustering with diverse transcription factors. Nat. Commun. *13*, 5703.

22. Sabari, B.R., Dall'Agnese, A., Boija, A., Klein, I.A., Coffey, E.L., Shrinivas, K., Abraham, B.J., Hannett, N.M., Zamudio, A.V., Manteiga, J.C., et al. (2018). Coactivator condensation at super-enhancers links phase separation and gene control. Science *361*, eaar3958.

23. Chong, S., Dugast-Darzacq, C., Liu, Z., Dong, P., Dailey, G.M., Cattoglio, C., Heckert, A., Banala, S., Lavis, L., Darzacq, X., et al. (2018). Imaging dynamic and selective low-complexity domain interactions that control gene transcription. Science *361*, eaar2555.

24. Kawasaki, K., and Fukaya, T. (2023). Functional coordination between transcription factor clustering and gene activity. Mol. Cell *83*, 1605–1622.e9.

25. Brangwynne, C.P., Eckmann, C.R., Courson, D.S., Rybarska, A., Hoege, C., Gharakhani, J., Jülicher, F., and Hyman, A.A. (2009). Germline P granules are liquid droplets that localize by controlled dissolution/condensation. Science *324*, 1729–1732.

26. Hnisz, D., Abraham, B.J., Lee, T.I., Lau, A., Saint-André, V., Sigova, A.A., Hoke, H.A., and Young, R.A. (2013). Super-enhancers in the control of cell identity and disease. Cell *155*, 934–947.

27. Bertrand, E., Chartrand, P., Schaefer, M., Shenoy, S.M., Singer, R.H., and Long, R.M. (1998). Localization of ASH1 mRNA particles in living yeast. Mol. Cell *2*, 437–445.

28. Spille, J.H., Hecht, M., Grube, V., Cho, W.K., Lee, C., and Cissé, I.I. (2019). A CRISPR/Cas9 platform for MS2-labelling of single mRNA in live stem cells. Methods *153*, 35–45.

29. Chakraborty, S., Kopitchinski, N., Zuo, Z., Eraso, A., Awasthi, P., Chari, R., Mitra, A., Tobias, I.C., Moorthy, S.D., Dale, R.K., et al. (2023). Enhancer-promoter interactions can bypass CTCF-mediated boundaries and contribute to phenotypic robustness. Nat. Genet. *55*, 280–290.

30. Brosh, R., Coelho, C., Ribeiro-Dos-Santos, A.M., Ellis, G., Hogan, M.S., Ashe, H.J., Somogyi, N., Ordoñez, R., Luther, R.D., Huang, E., et al. (2023). Synthetic regulatory genomics uncovers enhancer context dependence at the Sox2 locus. Mol. Cell *83*, 1140–1152.e7.

31. Li, Y., Rivera, C.M., Ishii, H., Jin, F., Selvaraj, S., Lee, A.Y., Dixon, J.R., and Ren, B. (2014). CRISPR reveals a distal super-enhancer required for Sox2 expression in mouse embryonic stem cells. PLoS One *9*, e114485.

32. Peng, T., Zhai, Y., Atlasi, Y., Ter Huurne, M., Marks, H., Stunnenberg, H.G., and Megchelenbrink, W. (2020). STARR-seq identifies active, chromatin-masked, and dormant enhancers in pluripotent mouse embryonic stem cells. Genome Biol. *21*, 243.

33. Zhou, H.Y., Katsman, Y., Dhaliwal, N.K., Davidson, S., Macpherson, N.N., Sakthidevi, M., Collura, F., and Mitchell, J.A. (2014). A Sox2 distal enhancer cluster regulates embryonic stem cell differentiation potential. Genes Dev. *28*, 2699–2711.

34. Alexander, J.M., Guan, J., Li, B., Maliskova, L., Song, M., Shen, Y., Huang, B., Lomvardas, S., and Weiner, O.D. (2019). Live-cell imaging reveals enhancer-dependent Sox2 transcription in the absence of enhancer proximity. eLife *8*, e41769.

35. Dekker, J., Rippe, K., Dekker, M., and Kleckner, N. (2002). Capturing chromosome conformation. Science *295*, 1306–1311.

36. Fudenberg, G., Abdennur, N., Imakaev, M., Goloborodko, A., and Mirny, L.A. (2017). Emerging evidence of chromosome folding by loop extrusion. Cold Spring Harb. Symp. Quant. Biol. *82*, 45–55.

37. Giorgetti, L., and Heard, E. (2016). Closing the loop: 3C versus DNA FISH. Genome Biol. *17*, 215.

38. Lieberman-Aiden, E., van Berkum, N.L., Williams, L., Imakaev, M., Ragoczy, T., Telling, A., Amit, I., Lajoie, B.R., Sabo, P.J., Dorschner, M.O., et al. (2009). Comprehensive mapping of long-range interactions reveals folding principles of the human genome. Science *326*, 289–293.

39. Mateo, L.J., Murphy, S.E., Hafner, A., Cinquini, I.S., Walker, C.A., and Boettiger, A.N. (2019). Visualizing DNA folding and RNA in embryos at single-cell resolution. Nature *568*, 49–54.

40. Fukaya, T., Lim, B., and Levine, M. (2016). Enhancer control of transcriptional bursting. Cell *166*, 358–368.

41. Chen, H., Levo, M., Barinov, L., Fujioka, M., Jaynes, J.B., and Gregor, T. (2018). Dynamic interplay between enhancer-promoter topology and gene activity. Nat. Genet. *50*, 1296–1303.

42. Benabdallah, N.S., Williamson, I., Illingworth, R.S., Kane, L., Boyle, S., Sengupta, D., Grimes, G.R., Therizols, P., and Bickmore, W.A. (2019). Decreased enhancer-promoter proximity accompanying enhancer activation. Mol. Cell *76*, 473–484.e7.

43. Chen, L.F., Lee, J., and Boettiger, A. (2023). Recent progress and challenges in single-cell imaging of enhancer-promoter interaction. Curr. Opin. Genet. Dev. *79*, 102023.

44. Gabriele, M., Brandão, H.B., Grosse-Holz, S., Jha, A., Dailey, G.M., Cattoglio, C., Hsieh, T.S., Mirny, L., Zechner, C., and Hansen, A.S. (2022). Dynamics of CTCF- and cohesin-mediated chromatin looping revealed by live-cell imaging. Science *376*, 496–501.

45. Ganji, M., Shaltiel, I.A., Bisht, S., Kim, E., Kalichava, A., Haering, C.H., and Dekker, C. (2018). Real-time imaging of DNA loop extrusion by condensin. Science *360*, 102–105.

46. Mirny, L., and Dekker, J. (2022). Mechanisms of chromosome folding and nuclear organization: their interplay and open questions. Cold Spring Harb. Perspect. Biol. *14*, a040147.

47. Hsieh, T.S., Cattoglio, C., Slobodyanyuk, E., Hansen, A.S., Darzacq, X., and Tjian, R. (2022). Enhancer-promoter interactions and transcription are largely maintained upon acute loss of CTCF, cohesin, WAPL or YY1. Nat. Genet. *54*, 1919–1932.

48. Rao, S.S.P., Huang, S.C., Glenn St Hilaire, B., Engreitz, J.M., Perez, E.M., Kieffer-Kwon, K.R., Sanborn, A.L., Johnstone, S.E., Bascom, G.D., Bochkov, I.D., et al. (2017). Cohesin loss eliminates all loop domains. Cell *171*, 305–320.e24.

49. Zuin, J., Dixon, J.R., van der Reijden, M.I., Ye, Z., Kolovos, P., Brouwer, R.W., van de Corput, M.P., van de Werken, H.J., Knoch, T.A., van IJcken, W.F., et al. (2014). Cohesin and CTCF differentially affect chromatin architecture and gene expression in human cells. Proc. Natl. Acad. Sci. USA *111*, 996–1001.

50. Aljahani, A., Hua, P., Karpinska, M.A., Quililan, K., Davies, J.O.J., and Oudelaar, A.M. (2022). Analysis of sub-kilobase chromatin topology reveals nano-scale regulatory interactions with variable dependence on cohesin and CTCF. Nat. Commun. *13*, 2139.

51. Alexander, K.A., Coté, A., Nguyen, S.C., Zhang, L., Gholamalamdari, O., Agudelo-Garcia, P., Lin-Shiao, E., Tanim, K.M.A., Lim, J., Biddle, N., et al. (2021). p53 mediates target gene association with nuclear speckles for amplified RNA expression. Mol. Cell *81*, 1666–1681.e6.

52. Kim, J., Venkata, N.C., Hernandez Gonzalez, G.A.H., Khanna, N., and Belmont, A.S. (2020). Gene expression amplification by nuclear speckle association. J. Cell Biol. *219*, e201904046.

53. Filippakopoulos, P., Qi, J., Picaud, S., Shen, Y., Smith, W.B., Fedorov, O., Morse, E.M., Keates, T., Hickman, T.T., Felletar, I., et al. (2010). Selective inhibition of BET bromodomains. Nature *468*, 1067–1073.

54. Kagey, M.H., Newman, J.J., Bilodeau, S., Zhan, Y., Orlando, D.A., van Berkum, N.L., Ebmeier, C.C., Goossens, J., Rahl, P.B., Levine, S.S., et al. (2010). Mediator and cohesin connect gene expression and chromatin architecture. Nature *467*, 430–435.

55. Kagey, M.H., Newman, J.J., Bilodeau, S., Zhan, Y., Orlando, D.A., van Berkum, N.L., Ebmeier, C.C., Goossens, J., Rahl, P.B., Levine, S.S., et al. (2011). Mediator and cohesin connect gene expression and chromatin architecture (vol 467, pg 430, 2010). Nature *472*, 247.

56. Fudenberg, G., Imakaev, M., Lu, C., Goloborodko, A., Abdennur, N., and Mirny, L.A. (2016). Formation of chromosomal domains by loop extrusion. Cell Rep. *15*, 2038–2049.

57. Alipour, E., and Marko, J.F. (2012). Self-organization of domain structures by DNA-loop-extruding enzymes. Nucleic Acids Res. *40*, 11202–11212.

58. Davidson, I.F., Barth, R., Zaczek, M., van der Torre, J., Tang, W., Nagasaka, K., Janissen, R., Kerssemakers, J., Wutz, G., Dekker, C., et al. (2023). CTCF is a DNA-tension-dependent barrier to cohesin-mediated loop extrusion. Nature *616*, 822–827.

59. Ilik, I.A., Malszycki, M., Lübke, A.K., Schade, C., Meierhofer, D., and Aktaş, T. (2020). SON and SRRM2 are essential for nuclear speckle formation. eLife *9*, e60579.

60. Sergé, A., Bertaux, N., Rigneault, H., and Marguet, D. (2008). Dynamic multiple-target tracing to probe spatiotemporal cartography of cell membranes. Nat. Methods *5*, 687–694.

61. Andrews, J.O., Conway, W., Cho, W.K., Narayanan, A., Spille, J.H., Jayanth, N., Inoue, T., Mullen, S., Thaler, J., and Cissé, I.I. (2018). qSR: a quantitative super-resolution analysis tool reveals the cell-cycle dependent organization of RNA polymerase I in live human cells. Sci. Rep. *8*, 7424.

62. Schindelin, J., Arganda-Carreras, I., Frise, E., Kaynig, V., Longair, M., Pietzsch, T., Preibisch, S., Rueden, C., Saalfeld, S., Schmid, B., et al. (2012). Fiji: an open-source platform for biological-image analysis. Nat. Methods *9*, 676–682.

63. Ershov, D., Phan, M.S., Pylvänäinen, J.W., Rigaud, S.U., Le Blanc, L., Charles-Orszag, A., Conway, J.R.W., Laine, R.F., Roy, N.H., Bonazzi, D., et al. (2022). TrackMate 7: integrating state-of-the-art segmentation algorithms into tracking pipelines. Nat. Methods *19*, 829–832.

64. Virtanen, P., Gommers, R., Oliphant, T.E., Haberland, M., Reddy, T., Cournapeau, D., Burovski, E., Peterson, P., Weckesser, W., Bright, J., et al. (2020). SciPy 1.0: fundamental algorithms for scientific computing in Python. Nat. Methods *17*, 261–272.

Please cite this article in press as: Du et al., Direct observation of a condensate effect on super-enhancer controlled gene bursting, Cell (2024), https://doi.org/10.1016/j.cell.2023.12.005

STAR★METHODS

KEY RESOURCES TABLE

REAGENT or RESOURCE	SOURCE	IDENTIFIER
Antibodies		
Goat Anti-Rabbit IgG H&L (Alexa Fluor® 647) preadsorbed	Abcam	Cat #: ab150083; RRID: AB_2714032
Rabbit anti-HA Tag Recombinant Monoclonal Antibody	Bethyl	Cat #: A191-102; RRID: AB_2891412
Recombinant Anti-beta Actin antibody [SP124] 500 uL	Abcam	Cat #: ab115777; RRID: AB_10899528
Anti-SMC3 antibody	Abcam	Cat #: ab9263; RRID: AB_307122
Goat Anti-Mouse IgG H&L (Alexa Fluor® 647)	Abcam	Cat #: ab150115; RRID: AB_2687948
Anti-SC35 antibody [SC-35] - Nuclear Speckle Marker	Abcam	Cat #: ab11826; RRID: AB_298608
Bacterial and virus strains		
NEB® 5-alpha Competent E. coli (High Efficiency)	NEB	C2987H
MAX Efficiency™ Stbl2™ Competent Cells	ThermoFisher	10268019
Chemicals, peptides, and recombinant proteins		
DMEM/F-12	ThermoFisher	11320033
Neurobasal™ Medium	ThermoFisher	21103049
N-2 Supplement (100X)	ThermoFisher	17502048
B-27™ Supplement (50X), serum-free	ThermoFisher	17504044
Penicillin-Streptomycin (10,000 U/mL)	ThermoFisher	15140122
AlbuMAX™ II Lipid-Rich BSA	ThermoFisher	11021029
MEM NEAA (100X)	ThermoFisher	11140050
Sodium Pyruvate (100 mM)	ThermoFisher	11360070
L-Glutamine (200 mM)	ThermoFisher	25030081
2-Mercaptoethanol	ThermoFisher	21985023
MEK inhibitor, PD0325910	Merck	PZ0162
GS GSK3β inhibitor, CHIR99021	Merck	SML1046
LIF Recombinant Mouse Protein	ThermoFisher	A35934
Poly-L-ornithine solution	Merck	P4957
Ultrapure Laminin, Mouse, 1 mg	Corning	354239
PBS - phosphate buffered saline (10x) pH 7.4, RNase free	ThermoFisher	AM9625
NEBuilder® HiFi DNA Assembly Master Mix	NEB	E2621
Lipofectamine™ 3000 Transfection Reagent	ThermoFisher	L 3000001
Super PiggyBac Transposase Expression Vector	System Biosciences	PB210PA-1
Puromycin dihydrochloride from *Streptomyces alboniger*	Merck	P8833
FastDigest BpiI (BbsI)	ThermoFisher	FD1014
T7 DNA Ligase	NEB	M0318
Janelia Fluor® HaloTag® Ligands, 646nm	Promega	GA1120
Janelia Fluor® HaloTag® Ligands, 549nm	Luke Lavis Lab	N/A
Paraformaldehyde 4% (w/v) in aqueous solution, methanol-free	VWR	47392.9M
Halt™ Protease Inhibitor Cocktail (100x)	ThermoFisher	78429
USB Dithiothreitol (DTT), 0.1M Solution	ThermoFisher	707265ML

(*Continued on next page*)

Please cite this article in press as: Du et al., Direct observation of a condensate effect on super-enhancer controlled gene bursting, Cell (2024), https://doi.org/10.1016/j.cell.2023.12.005

Continued

REAGENT or RESOURCE	SOURCE	IDENTIFIER
Leibovitz's L-15 Medium, no phenol red	ThermoFisher	21083027
TrypLE ™ Express Enzyme (1x), phenol red	ThermoFisher	12605028
Opti-MEM ™ I Reduced Serum Medium, no phenol red	ThermoFisher	11058021
Triton X-100	Merck	T8787-250ML
BSA	Merck	A9418-50G
Deposited data		
tcPALM data_Original_Cell_Line	This study	Zenodo data: https://doi.org/10.5281/zenodo.10220085
tcPALM data_CTCF_E-2_deletion	This study	Zenodo data: https://doi.org/10.5281/zenodo.10221545
tcPALM data_E15_deletion	This study	Zenodo data: https://doi.org/10.5281/zenodo.10222551
tcPALM data_SCR_deletion	This study	Zenodo data: https://doi.org/10.5281/zenodo.10222721
tcPALM data_Cohesin_depletion	This study	Zenodo data: https://doi.org/10.5281/zenodo.10223195
SIM_data	This study	Zenodo data: https://doi.org/10.5281/zenodo.10219682
Lattice light sheet data	This study	Zenodo data: https://doi.org/10.5281/zenodo.10219582
Experimental models: Cell lines		
R1 mouse embryonic stem cells	Eliezer Calo Lab, MIT	N/A
Dendra2-Pol II/Halo-Mediator	Cho et al.[16]	N/A
Dendra2-Pol II/Halo-Mediator/ MCP-SNAP/Sox2-24xMS2	This study	N/A
Dendra2-Pol II/Halo-Mediator/MCP-SNAP/ Sox2-24xMS2/SMC3-FKBP12F36V	This study	N/A
Dendra2-Pol II/Halo-Mediator/MCP-SNAP/ Sox2-24xMS2/ Δ(CTCF/E_{-2})	This study	N/A
Dendra2-Pol II/Halo-Mediator/ MCP-SNAP/Sox2-24xMS2/ ΔE_{+15}	This study	N/A
Dendra2-Mediator/Halo-Pol II/ MCP-SNAP/Sox2-24xMS2	This study	N/A
Sox2 enhancer(CuO/CymR)/Halo-Mediator/ MCP-SNAP/Sox2-24xMS2	This study	N/A
Sox2 enhcancer(CuO/CymR)/Halo-Pol II/ MCP-SNAP/Sox2-24xMS2	This study	N/A
Sox2 enhancer(CuO/CymR)/Halo-Mediator/ MCP-SNAP/Sox2-24xMS2/ Δ(CTCF/E_{-2})	This study	N/A
Sox2 enhancer(CuO/CymR)/Halo-Mediator/ MCP-SNAP/Sox2-24xMS2/ ΔE_{+15}	This study	N/A
Sox2 enhancer(CuO/CymR)/Halo-Mediator/ MCP-SNAP/Sox2-24xMS2/ ΔSCR	This study	N/A
Oligonucleotides		
ssDNA for Bxb1 site insertion	IDT	N/A
Recombinant DNA		
Plasmid: P162_pX459-Rbp1_sgRNA2	Cho et al.[16]	N/A
Plasmid: P153_pX459-Med19_sgRNA1	Cho et al.[16]	N/A
Plasmid: B00126(stable expression for MCP-SNAP)	This study	N/A
Plasmid: pX330-Sox2gRNA	This study	N/A
Plasmid: pX330-Smc3gRNA	This study	N/A
Plasmid: pX458-CuOgRNA	This study	N/A
Plasmid: Sox2-MS2 Repair Template	This study	N/A
Plasmid: SMC3-FKBP12F36V Repair Template	This study	N/A
Plasmid: Sox2-MS2 Repair Template	This study	N/A
Plasmid: Sox2-MS2 Repair Template	This study	N/A

(*Continued on next page*)

Continued		
REAGENT or RESOURCE	SOURCE	IDENTIFIER
Plasmid: UBCpr-CymR-EGFP	This study	N/A
Plasmid: pX330-gRNA1-CTCF_E$_{-2}$	This study	N/A
Plasmid: pX330-gRNA2-CTCF_E$_{-2}$	This study	N/A
Plasmid: pX330-gRNA1-E$_{+15}$	This study	N/A
Plasmid: pX330-gRNA2-E$_{+15}$	This study	N/A
Plasmid: pX330-gRNA1-SCR	This study	N/A
Plasmid: pX330-gRNA2-SCR	This study	N/A
Plasmid: CTCF_E$_{-2}$-BSD RT	This study	N/A
Plasmid: E$_{+15}$-BSD RT	This study	N/A
Plasmid: SCR-BSD RT	This study	N/A
Software and algorithms		
MATLAB	MathWorks	https://www.mathworks.com/products/matlab.html
ImageJ	NIH	https://imagej.nih.gov/ij/
Benchling	Benchling Inc.	https://www.benchling.com/
GraphPad Prism 9	GraphPad Software, LLC	https://www.graphpad.com/
Python	Open source	https://www.python.org/
Lattice light sheet analysis software	This study	Zenodo data: https://doi.org/10.5281/zenodo.10200779
Other		
Nalgene™ Sterile Syringe Filters (0.45 μm)	ThermoFisher	725-2545
35mm Dish, Uncoated, Coverslip No.1.5, 20mm Glass Diameter	MatTek	P35G-1.5-20-C
500cm^2 Square TC-treated Culture Dish	Corning	431110
Cell Scrapers and Lifters	Corning	3008

RESOURCE AVAILABILITY

Lead contact

Further information and requests for resources and reagents should be directed to and will be fulfilled by the lead contact, Ibrahim I. Cissé (cisse@ie-freiburg.mpg.de).

Materials availability

- All plasmids and cell lines generated in this study are available from the lead contact upon request, and will be distributed with MTA.
- This study did not generate new unique chemical reagents.

Data and code availability

- Microscopy data reported in this paper has been deposited at Zenodo and is publicly available as of the date of publication. DOIs are listed in the key resources table.
- All original code has been deposited at Zenodo and is publicly available as of the date of publication. DOIs are listed in the key resources table.
- Any additional information required to reanalyze the data reported in this paper is available from the lead contact upon request.

EXPERIMENTAL MODEL AND SUBJECT DETAILS

All mouse embryonic cell lines used in this study are listed in key resources table.

METHOD DETAILS

Mouse embryonic stem cell (mESC) culture

All cell lines used in this study were based on R1 Mouse embryonic stem cells (mESCs). Cells were cultured in serum-free 2i media without feeder MEF cells (1:1 of DMEM/F-12 and Neurobasal media, supplemented with 1x N-2 supplement, 1x B-27 supplement, 100 U/ml PenStrep, 3 μg/ml AlbuMAX™ II, 1x MEM NEAA, 1mM Sodium pyruvate, 1mM L-glutamine (all from Thermo Fisher Scientific), 0.1 μM 2-Mercaptoethanol (Sigma-Aldrich), 1mM MEK inhibitor (PD0325910, Stemgent), 3mM GSK3β inhibitor (CHIR99021, Stemgent) and 100 U/ml LIF (Leukemia Inhibitory Factor, EMD Millipore). All the flasks or petri dishes were coated with 5 μg/ml poly-Lornithine (PLO, Sigma) in 1x PBS buffer in 37°C for more than 5 hours, followed by 5 μg/ml Laminin (VWR) in 1x PBS buffer with >5 hours incubation in 37°C to prepare for stem cell culture. The cells were grown in a 37°C incubator maintaining 5% CO_2 in a water-saturated atmosphere. Cell culture media were exchanged every 24 hours. Pluripotency of mESC was checked periodically by alkaline phosphatase (AP) expression level using Alkaline Phosphatase Live Stain Kit (Thermo Fisher Scientific), and by cell phenotype.

mESC cell line engineering

Crispr-cas9 editing of endogenous RNA Pol II and Med19 with Dendra2 or Halo

sgRNAs targeting +/- 100 bps around the start codons of the Rbp1 and Med19 genes were designed using the benchling CRISPR tool, and cloned into px330. Repair templates are synthesized through GeneArt services by ThermoFisher. We used the same plasmids and followed a previously published protocol for endogenous RNA Pol II and Mediator tagging.[16]

Generating Sox2-T2A-PuroR-24xMS2 Cell Line

A repetitive DNA region encoding 24 MS2 stem loop repeats (24xMS2) was knocked into the 3' untranslated region (UTR) of the endogenous mouse SRY-box 2 (*Sox2*) using a CRISPR/Cas9 system by cleaving a DNA region after *Sox2* exon 1 (ENSMUSG00000074637). A single-guide RNA (TGGCCGAATGATTAATAACG) was inserted to pSpCas9(BB)-2A-Puro (PX459) V2.0 (a gift from Feng Zhang (Addgene plasmid # 62988; http://n2t.net/addgene:62988; RRID:Addgene_62988)). Sox2-T2A-PuroR-24xMS2 repair template plasmid was engineered as reported previously.[28] The middle of homology arms of around 800 base-pairs on each side of the cleavage site contains a DNA region encoding T2A-PuroR-24xMS2. The circular repair template plasmid and the sgRNA-Cas9 plasmid were co-transfected into mESCs with a ratio of 3 to 2. Three days after transfection, cells were selected by puromycin (2 ug/ml) incubation for 7 days. Then, single cells were sorted by FACS. One or two weeks after FACS, surviving sorted cells were incubated with 100 nM JF646-SNAPtag ligand for 10 min and washed for 30 min, and imaged by microscope to select cells showing vivid MS2 foci in nucleus.

Stable Expression of NLS-MCP-SNAP in ES cell lines

EF1a-NLS-2xMCP-SNAP plasmid was engineered as reported previously. This plasmid was transfected using Lipofectamin 3000 (Thermo Fisher Scientific, L3000001) into mouse embryonic stem cells with 70-80% confluency in a 6-well. One day after transfection, half of the cells were transferred to T75 for growth. Three days after transfection, cells were firstly split using TrypLE (Thermo Fischer Scientific, 12605010) and centrifuged down at 900 rpm for 2 min. After removing supernatant, cells were incubated with 100 nM JF646-SNAPtag ligand (A gift from L. D. Lavis (HHMI, Janelia)) for 10 min and washed for 15 min. Then, single cells with positive JF646 signals were sorted into a 96-well plate by FACS. One or two weeks after FACS, surviving sorted cells were transferred into glass-bottom imaging dishes (Mattek, P35-1.5-20-C) and incubated with 100 nM JF646-SNAPtag ligand for 10 min for microscope test. Under 642 nm illumination, only cells showing stable JF646 signals were selected for the further experiments.

Crispr-cas9 editing of endogenous Smc3 with FKBP12^{F36V}

sgRNA targeting ± 100 bps around the stop codon of the *Smc3* gene (ENSMUST00000025930) was designed using the benchling CRISPR tool, and cloned into px330(gRNA sequence: GTAGAAGACGATACCACGCA). Repair templates are synthesized through GeneArt services by ThermoFisher. Cells were cultured on 6-well dishes to a confluency of 70%-80%, and the circular repair template plasmid containing homology arms of Smc3 and FKBP12^{F36V}-HA-P2A-BFP and the sgRNA-Cas9 plasmid were co-transfected into mESCs with a ratio of 3 to 2. Three days after transfection, single cells were sorted by FACS on BFP positive signals. One or two weeks after FACS, surviving sorted cells were tested by genomic DNA extraction and PCR, followed by western blot to check the dTAG degradation efficiency.

Crispr-cas9 editing of deletion of CTCF/E$_{-2}$, E$_{+15}$, and SCR sites

sgRNAs targeting CTCF/E_{-2}, E_{+15} and SCR regions were designed and cloned into px330. Repair templates are synthesized through GeneArt services by ThermoFisher. Cells were cultured on 6-well dishes to a confluency of 70%-80%, and the circular repair template plasmid containing homology arms of sequences ± 800 bps flanking the designed deletion sites and a blasticidin selection marker driven by the EF1alpha promoter, and two sgRNA plasmids targeting the 5' and 3' region of the designed deletion site were transfected into the 6-well. The next day, cells were splitted into T75 flasks and grow for two more days before adding 5ug/ml blasticidin for selection. The clones were under selection for a week and then sorted into monoclones by FACS and subsequently genotyped by PCR. The genomic coordinates for each designed deletion are: ΔCTCF/E_{-2} (chr3:34685603:34702495), ΔE_{+15} (chr3: 34722279: 34723439), and ΔSCR (chr3: 34786930: 34819951). The coordinate annotations are referenced to GRCm39.

Confirmation of deletions of CTCF/E$_{-2}$, E$_{+15}$, and SCR sites

We designed primers and performed PCR assays to check whether our deletions are as desired (Figure S6). In each cell line, we extracted the genomic DNA using standard NEB genomic DNA preparation kit and performed three tests (left junction PCR, right junction PCR and zygosity test). The primer sequences are listed here:

P1(gaagttcagaggcatcttcag), P2(gccagctgccgcagcagcagcag), P3(gggggaccttgtgcagaactcg), P4(ccttccactctcttgttggaac), P5(cagtttgtaaggacaatgag), P6(ccttctgagaacattatcgag), P7(cggcagtcccctaagctttg), P8(cgtagtctgttgtcctaagc), P9(gcccaaactggcttgtacctc), P10(cccctagtacttccaagtagc), P11(gataaaccaccccatatata).

For CTCF/E_{-2} deletion, P1/P2 were used for left junction PCR, and P3/P4 were used for right junction PCR. The expected band lengths are 879bp and 995bp respectively. To test zygosity, we used two sets of primers P1/P4 and P5/P4 for PCR. For homozygous deletion, we expect a band of 1.8kb in P1/P4 PCR, and no band in P5/P4 PCR.

For E_{+15} deletion, P6/P2 were used for left junction PCR, and P3/P7 were used for right junction PCR. The expected band lengths are 827bp and 854bp respectively. To test zygosity, we first used primers P6/P7 for PCR. Since the deleted region is replaced with the blasticidin marker with a very similar length, we carried an additional NdeI digestion to differentiate from the non-deleted allele if it's heterozygous deletion. For homozygous deletion, we expect a band of 1.8kb in P6/P7 PCR, and the purified 1.8kb band should be digested into 1.5kb and 300bp without remaining 1.8kb. If heterozygous deletion, there should be digested bands 1.5kb and 300bp, and also the remaining 1.8kb.

For SCR deletion, P8/P2 were used for left junction PCR, and P3/P9 were used for right junction PCR. The expected band lengths are 1049bp and 1061bp respectively. To test zygosity, we used two sets of primers P8/P9 and P10/P11 for PCR. For homozygous deletion, we expect a band of 1853bp in P8/P9 PCR, and no band in P10/P11 PCR. If it's heterozygous deletion, there is a band of 1853 bp in P8/P9 PCR and also a band of 285 bp in P10/11 PCR. We were only able to get heterozygous deletion for SCR, possibly due to lethality after SCR deletion in 2i culturing condition.

CuO array insertion by Bxb1 and PhiC31 integrases

For integration of the CuO array 5Kb downstream of *Sox2* control region, we followed the strategy by Alexander et al. (Figure S2E).[34] We first transfected 1ug of a px458 plasmid containing the gRNA sequence (GTAAGCTATCTCATTGCCCG) together with 1.5ug of a doner ssDNA repair template containing Bxb1 attp sequence through lipofectamine. After three days of transfection, cells were FACS sorted into monolones in 96-well plate and later checked by gDNA PCR test. The selected clone was then transfected with 2.5 ug of a plasmid bearing the Bxb1/attB sequence for homologous recombination, the 144X CuO repeats and a puromycin resistance cassette flanked by loxp sites which can be flopped upon expression of Cre protein. The cells were grown for three days and selected under 4ug/ml puromycin for a week before FACS sorting. The monoclones were then checked with PCR as well as imaging after another transfection of UBCpr-CymR-EGFP plasmid (Figure S2F). The correct monoclone which contains the 144X CuO array was then transfected with a plasmid expressing Cre protein to pop out puromycin selection cassette in order to reduce the effect of long insertion next to the *Sox2* SCR region.

Antibody staining of nuclear speckles

Cells were seeded on the Mattek imaging dish a day before, and incubated with 100nM JF549 Halo ligand to stain the Mediator or Pol II clusters for 90 min and washed with 2i media, followed by 30 min incubation in 2i media without ligands. Cells growing on the imaging dishes were gently washed three times with ice-cold 1x PBS, followed by 4% PFA for 10 min at room temperature. After three times washing with ice-cold 1x PBS, cells were permeabilized with 0.25% Triton X-100 in 1x PBS for 5 min at room temperature. After three times washing with ice-cold 1x PBS, cells were incubated with 2% (w/v) BSA in 1x PBS at 4°C for 1 hour, followed by incubation with Anti-SC35 primary antibody(1:200 dilution) in 2% BSA at 4°C overnight. After three times washing with ice-cold 1x PBS, cells were incubated with Goat Anti-Mouse IgG H&L (Alexa Fluor® 647) secondary antibody(1:1000 dilution) in 2% BSA 4°C for 1 hour, followed by three times washing with ice-cold 1x PBS for imaging. We note that SRRM2 (Serine/arginine repetitive matrix protein 2) is the primary target of mAb SC35,[59] which is a marker for nuclear speckles.

Live-cell Photoactivated localization microscopy (PALM)

Live cell PALM imaging was carried out as described before.[16] mESCs used for live cell PALM imaging was derived from R1 background, with *Sox2* gene tagged by 24 repeats of MS2 at its 3' UTR, Rpb1 tagged with Dendra2 at its N terminal, EF1α-NLS-MCP-SNAP stably expressed in the cell, and both alleles of *SMC3* tagged with a degradation sensitive $FKBP^{F36V}$ tag. Cells were simultaneously illuminated with 1.3 W/cm2 near UV light (405nm) for photo-conversion of Dendra2 and 2.1 kW/cm2 (561nm) for fluorescence detection with an exposure time of 50ms. We acquired images of Dendra2- RNA Pol II for 120s (2400 frames) for quantification of RNA Pol II clusters. For dual color imaging, cells were incubated with 100nM JF646 SNAP ligand for 90 min and washed with 2i media, followed by 30 min incubation in 2i media without JF646-SNAPTag ligands, to wash out unbound SNAP ligands before fluorescence imaging in L-15 medium. We acquired a snapshot of MS2 channel with 642nm excitation with a power intensity of 2.5 kW/cm2 and quickly switched to simultaneous 405/561 imaging for PALM. For cohesin depletion experiments, DMSO or dTAG13 (500nM) was added together with the dyes during the staining process and kept in L-15 during imaging to maintain the degradation condition. Considering the staining and image acquisition time, the total treatment time of dTAG13 is four hours.

Lattice light sheet imaging

Cells were plated on 35mm MatTek imaging dishes (No. 1.5 coverslip, coated with PLO and laminin) one day before the experiment, and reach the 70-80% confluency next day. Cells were incubated with 100nM JF646-SNAP dye and JF549-Halo dye for 90 min and washed with 2i media, followed by 30 min incubation in 2i media without JF646-HaloTag ligands, to wash out unbound SNAP ligands before fluorescence imaging in L-15 medium. Directly before imaging, the medium was changed to L-15 medium. For Cohesin depletion experiments, DMSO or dTAG13 (500nM) was added together with the dyes during the staining process and kept in L-15 during imaging to maintain the degradation condition. Considering the staining and image acquisition time, the total treatment time of dTAG13 is four hours in the cohesin depletion condition. Data were acquired on a ZEISS Lattice Lightsheet 7 microscope, using light-sheet Sinc3 30x1000. Excitation wavelengths were 561nm and 640nm for two color experiments, and 488nm/561nm/640nm for three color experiments. The emission filter was set to the following wavelengths: 420–470, 503–546, 576–617, 656–750. 3D Image stacks were acquired by moving the sample stage through the light sheet with a step size of 0.3 μm, and time interval between each 3D scan is 30s. Total image acquisition time is 20-30min. The laser power was set at 8% for 488nm illumination, 40% for 561nm laser, and 40% for the 642nm. Pixel size is 145nm.

Structured illumination microscopy

Cells were plated on 35mm MatTek imaging dishes as described above. Cells were incubated with 100nM JF646-SNAP dye and JF549-Halo dye for 90 min and washed with 2i media, followed by 30 min incubation in 2i media without JF646-HaloTag ligands, to wash out unbound SNAP ligands before fluorescence imaging in L-15 medium. Cells were then imaged with the Zeiss Elyra 7 lattice SIM,[2] and the laser intensity of 488nm, 561nm, and 642nm are 2%, 4%, and 2% respectively with an exposure time of 100ms. The SIM pattern used is 27.5μm (488nm channel), 27.5μm (561nm channel), and 32μm(642nm channel) with 13 phases. A z-stack of 11 slices with 0.3 μm interval was acquired for each region of interest. Images were analyzed using the standard Zeiss SIM processing algorithm and projected in xy with maximum intensity. Objects were then identified in Fiji and the size of the condensate was calculated as the average Feret's diameter (mean diameter between the shortest and longest axis).

QUANTIFICATION AND STATISTICAL ANALYSIS

tcPALM analysis

Super-resolution images were reconstructed and analyzed using MTT[60] and qSR.[61] We generated a rendered super-resolution image by placing Gaussian peaks with spread corresponding to the localization accuracy (50 nm) at the position of single molecule localizations. We then identified clusters in PALM images using qSR. To localize MS2 spots, we subtracted background (Median filtered original image with 5 pixel radius and subtract Gaussian filtered image with 9 pixel radius) and adjusted the contrast to remove fluorescence background in the nucleus which is higher than background in the cytoplasm. We resized super-resolution images and merged with *Sox2* MS2 channel in Fiji. The distance is calculated as the distance between the centroid of the *Sox2* MS2 nascent transcription site and the centroid of the nearest Pol II cluster. Nascent RNA transcript level is quantified by dividing the integrated intensity of MS2 spot divided by the mean integrated intensity of all the single mRNAs.

Quantification of burst size, burst frequency, total fraction of mRNA

We quantified the burst size in each single cell as the count of mRNA produced at the time when tcPALM images were taken. We first identified the nascent *Sox2* transcription spot (brightest spot in the nucleus), and measured the integrated intensity inside a 7x7 pixel square window centered at the spot. Background intensity per pixel was calculated by subtracting integrated intensity of a larger 9X9 window centered at the spot with the integrated intensity of the 7X7 window and then divided by the number of pixels in the square ring. The spot intensity is then calculated as the total integrated intensity within the 7X7 window minus total background intensity within the 7X7 window. The same quantification is done for single mRNAs in the cytoplasm. We averaged all integrated intensity of single RNAs to get a mean integrated intensity. Burst size is then calculated by dividing the integrated intensity of MS2 spot by the mean integrated intensity of single mRNAs.

We calculate burst frequency as the fraction of bursting events occurred with a proximal or distal cluster in our tcPALM data. The total fraction of mRNA produced in proximal is calculated as the integrated total number of mRNA from proximal data points (< 1 μm) divided by the integrated total number of mRNA from all data points. The total fraction of mRNA produced in distal is calculated as the integrated total number of mRNA from distal data points (> 1 μm) divided by the integrated total number of mRNA from all data points.

Condensate size measurement

In all cell lines, we measured the Mediator condensate sizes in Fiji using the structured illumination microscopy data. We used both CuO labels and bursting *Sox2* mRNA signals as indications to identify the nearest condensate to both CuO and *Sox2* locus. We manually identified the nearest Mediator condensate that is within 3 μm from CuO and *Sox2* locus, and measured the minimum and maximum Feret's diameter of that condensate region, and calculated the average between minimum and maximum Feret's diameter to get the condensate diameter measurement. For the enhancer deletion cell lines, more data were taken since the fraction of bursting cells with a *Sox2* mRNA signal is reduced.

Lattice light sheet imaging analysis

Maximum intensity projections were created in ZEISS Zen Blue software. Regions of interest around individual cells, which were manually identified to show a burst of MS2 signal, were cropped. The data was then bleach corrected by exponential fitting of intensities in each channel in Fiji,[62] and background subtracted, by subtracting a median filtered image (radius 9 px) from the bleach corrected image in Fiji.

To obtain rough position estimates of CuO, Med/RNA Pol II, and MS2 spots, we used TrackMate in Fiji was used for semi-automatic tracking, by manually selecting foci and verifying all tracks.[63] These coordinate estimates were used in a Gaussian fitting procedure in Python. A 2D Gaussian

$$i(x,y) = a \exp\left(-\frac{(x-x_0)^2}{2\sigma_x^2} - \frac{(y-y_0)^2}{2\sigma_y^2}\right) + c,$$

Please cite this article in press as: Du et al., Direct observation of a condensate effect on super-enhancer controlled gene bursting, Cell (2024), https://doi.org/10.1016/j.cell.2023.12.005

where a is the intensity at the peak and c the background fluorescence, was fitted (using scipy.optimize.curvefit[64]) to a 15x15 pixel region around the guessed spot position. The maximum intensity pixel in the center third of the 15x15 ROI was used as the initial parameter for the peak position $x0$, $y0$. The maximum and mean intensity inside the ROI were used as initial paramaters for the peak height a and background c, respectively.

After fitting, each frame was classified as to whether a true signal is present or not, according to manually determined thresholds:

- Minimum R^2 of the fit: $R^2 > 0.12$
- Maximum x- and y-variance: $\sigma_x^2 < 25$, $\sigma_y^2 < 25$
- Minimum relative intensity: $a/c > 3.4$
- Minimum signal duration of 4, meaning that each signal positive frame has to be followed by at least 3 signal positive frames.

For each frame that passes these thresholds, we stored a position as the coordinates of the Gaussian peak $x0$, $y0$, and an intensity I as the integral of the Gaussian

$$\begin{aligned} I &= \int_{-\infty}^{\infty}\int_{-\infty}^{\infty}(i(x,y) - c)\mathrm{d}x\mathrm{d}y \\ &= a\int_{-\infty}^{\infty}\int_{-\infty}^{\infty}\exp\left(-\frac{(x-x_0)^2}{2\sigma_x^2}\right)\exp\left(-\frac{(y-y_0)^2}{2\sigma_y^2}\right)\mathrm{d}x\mathrm{d}y \\ &= 2\pi a\sqrt{\sigma_x^2\sigma_y^2}. \end{aligned}$$

For frames that do not pass the thresholds, or if the fit was unsuccessful, the intensity is set to a background value, as the mean intensity inside the 15x15 ROI. The coordinates and intensities are then used for further analysis.

Supplemental figures

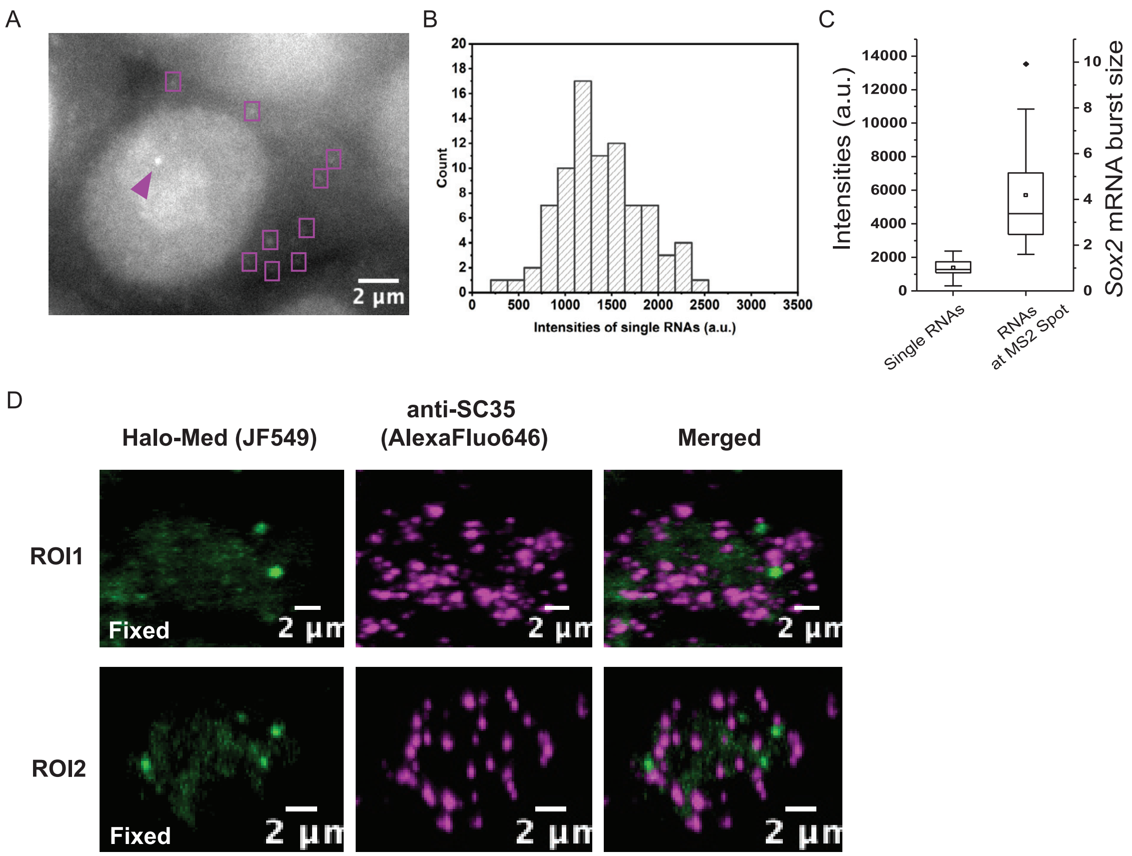

Figure S1. Quantification of *Sox2* mRNA burst sizes and antibody staining of nuclear speckles and condensates, related to Figure 1

(A) Representative image showing single diffusing *Sox2* MS2 nascent mRNA (magenta box) in the cytoplasm and multiple *Sox2* mRNAs associated at the native transcription site (MS2 spot, indicated by magenta arrow). Scale bars, 2 µm.

(B) Histogram of intensities of single *Sox2* mRNAs shows a gaussian distribution. Mean intensity is at 1,382 arbitrary unit.

(C) Measurement of *Sox2* burst size at MS2 spots in 30 cells based on normalization to the mean intensity of 83 single *Sox2* mRNAs.

(D) Antibody staining of nuclear speckles shows the transcriptional condensates are not nuclear speckle condensates. Dual color imaging of Halo-Mediator (Janelia Fluor 549) and anti-SC35 (nuclear speckle marker, stained by Alexa Fluor 646 secondary antibody) shows no colocalization between condensates (Mediator as a marker) and nuclear speckles. Mediator is shown in green (left), SC35 is shown in magenta (middle) and merged images are shown in the right panel. Note that anti-SC35 primary antibody was reported to mainly stain against SRRM2, a marker for nuclear speckles.

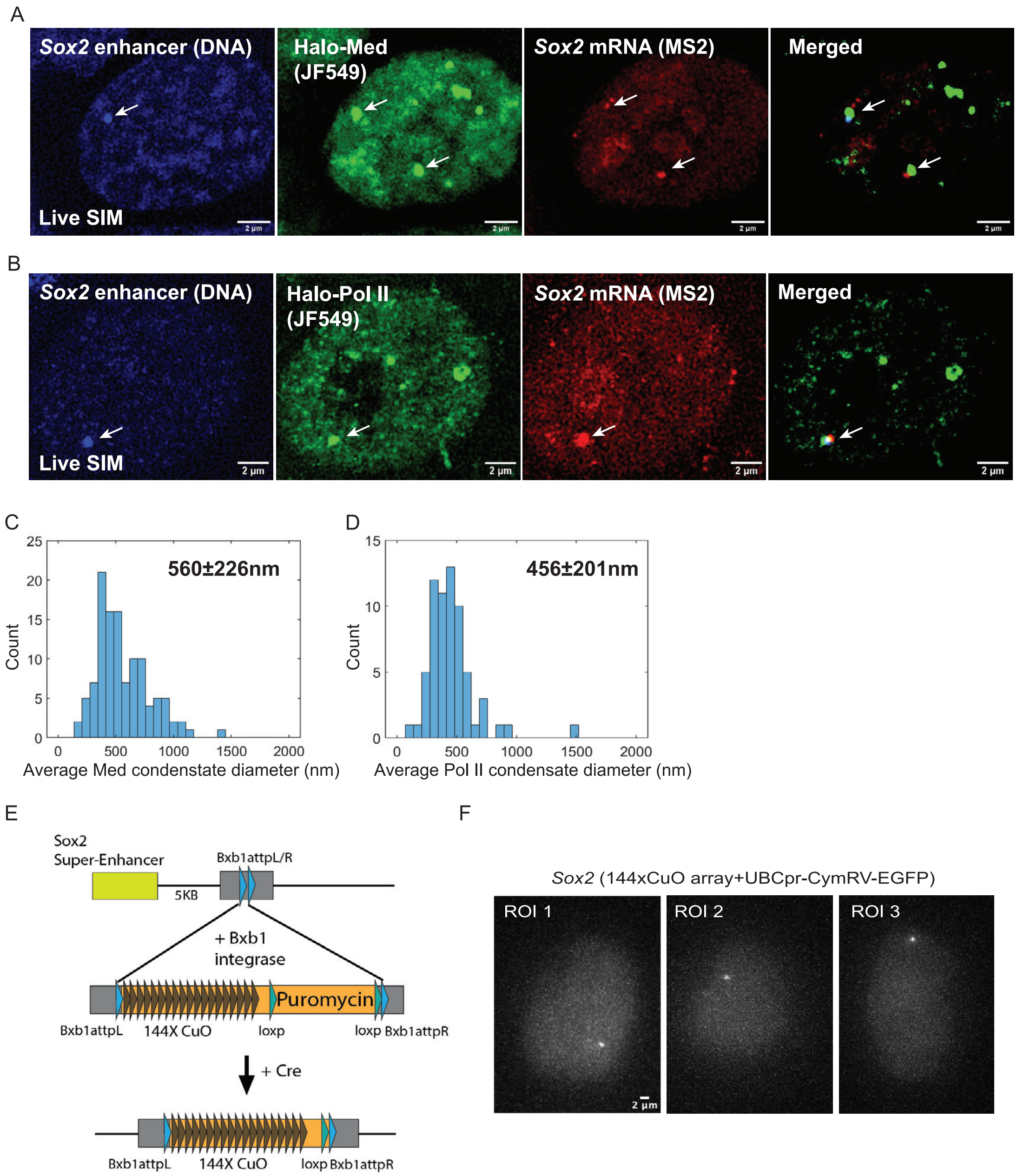

Figure S2. Quantification of condensate sizes (RNA Pol II and Mediator) by live-cell SIM, related to Figures 2 and 4 and STAR Methods

(A) Three-color live SIM imaging of *Sox2* super-enhancer (labeled by a CuO array, first left), condensate (Halo-Mediator labeled by JF_{549}, second left) and *Sox2* mRNA (second right), and merged (first right). Arrow indicates where the actively bursting gene is located. Both *Sox2* alleles of this cell line is tagged and bursting in the example shown.

(B) Three-color live SIM imaging of *Sox2* super-enhancer (first left), condensate (Halo-RNA Pol II labeled by JF_{549}, second left), and *Sox2* mRNA (second right), and merged (first right). Scale bars, 2 μm.

(C) Histogram of condensate (Mediator as a marker) size. Condensate size is calculated as the average Feret's diameter (mean diameter between the shortest axis and longest axis). Mean ± standard deviation is 560 ± 226 nm.

(D) Histogram of condensate (RNA Pol II as a marker) size. Mean ± standard deviation is 456 ± 201 nm.

(E) Schematic for insertion of a 144× CuO array at the *Sox2* canonical super-enhancer site by using a three-step strategy developed by Alexander et al.[34] An attpL/R site was inserted 5 kb downstream of the canonical *Sox2* enhancer site through CRISPR-CAS9 method. A plasmid containing 144× CuO sites and expressing Bxb1 integrase was transfected and integrated the CuO array at the attpL/R site through recombination. A second plasmid expressing the Cre recombinase was transfected and will cut out the selection marker puromycin through *loxp* sites.

(F) Validation of successful 144× CuO labeling of the *Sox2* super-enhancer region by imaging. Cells were transfected with a plasmid expressing CymR-EGFP which binds to CuO sites and will mark the chromatin locus as a dot in the nucleus. Scale bars, 2 μm.

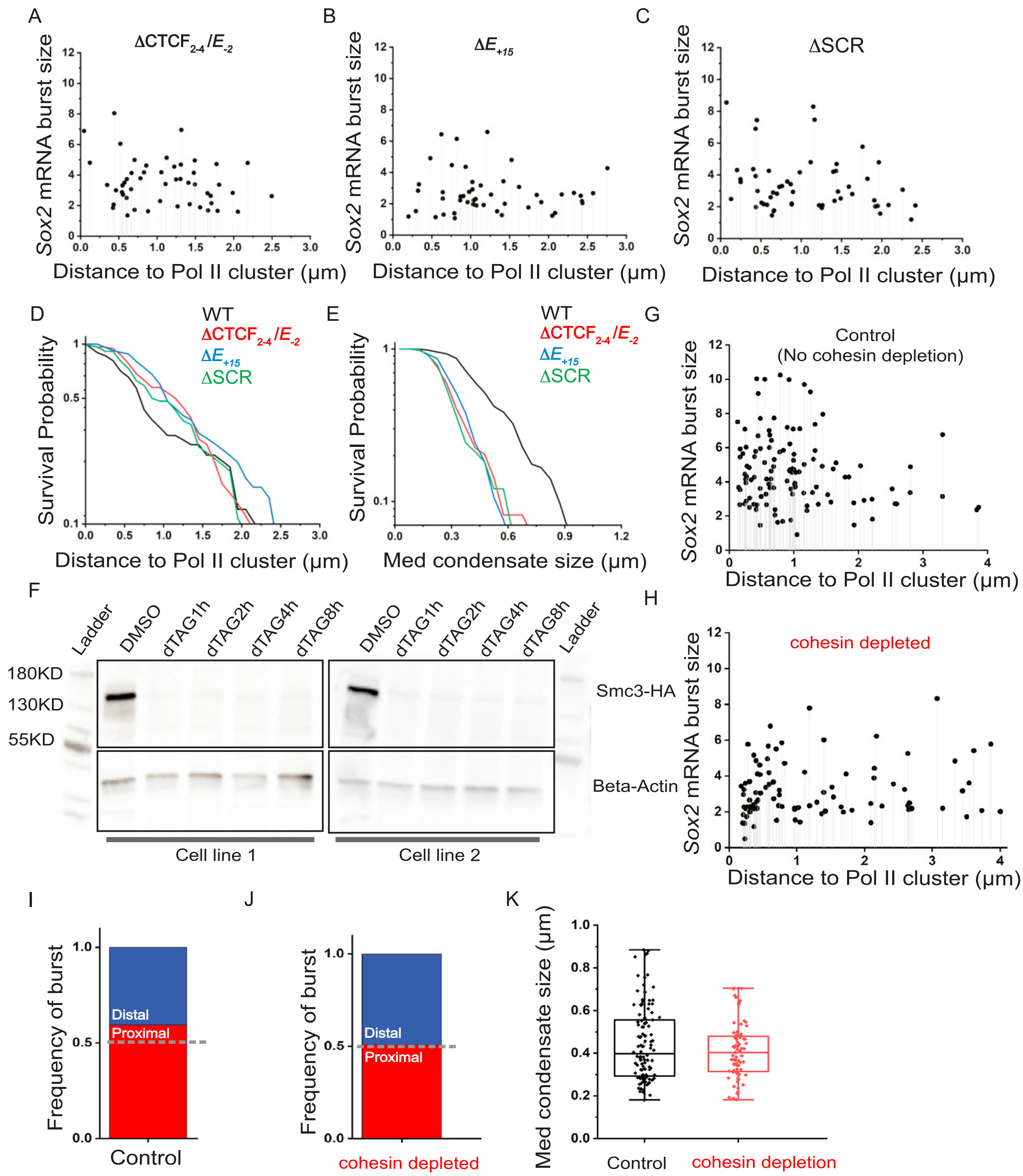

Figure S3. CTCF/E$_{-2}$, E$_{+15}$, and SCR deletions abolish condensate based burst enhancement, related to Figures 2 and 5

(A) Plot of *Sox2* mRNA burst size vs. the distance between the nearest RNA Pol II cluster to the *Sox2* locus shows no proximity-based gene bursting enhancement in CTCF/E$_{-2}$ deleted cell line. The threshold to define proximal and distal clusters is set arbitrarily at 1 μm. The distance is calculated as the centroid-to-centroid distance of the MS2 signal and the nearest persistent RNA Pol II cluster in the rendered image.

(B) Plot of *Sox2* mRNA burst size vs the distance between the nearest RNA Pol II cluster to the *Sox2* locus in E$_{+15}$ deleted cell line.

(C) Plot of *Sox2* mRNA burst size vs. the distance between the nearest RNA Pol II cluster to the *Sox2* locus in SCR deleted cell line.

(D) Survival probability plot of distance-to-RNA Pol II cluster distributions in wild-type (black curve), ΔCTCF/E$_{-2}$ (red curve), ΔE$_{+15}$ (blue curve), and ΔSCR (green curve) cell lines.

(E) Survival probability plot of condensate sizes (Mediator) in wild-type (black curve), ΔCTCF/E$_{-2}$ (red curve), ΔE$_{+15}$ (blue curve), and ΔSCR (green curve) cell lines. Both survival probability plots in (D) and (E) are calculated as 1-probability$_{cumulative}$ and plotted in log linear scale.

(F) Western blot data shows a validation of rapid degradation of SMC3 protein. The left 5 lanes beside protein ladder are from the cell line 1: Dendra2-RNA Pol II/Halo-Mediator/*Sox2*-24xMS2/MCP-SNAP/SMC3-FKBP12^{F36V}, and the right 5 lanes are from the cell line 2: CuO (labeling *Sox2* enhancer)/Halo-RNA Pol II/*Sox2*-24xMS2/MCP-SNAP/SMC3-FKBP12$_{F36V}$. The upper panel is HA tagged Smc3 proteins using anti-HA antibody, and the lower panel is anti-β-actin as a loading control.

(legend continued on next page)

(G) Plot of *Sox2* mRNA burst size vs. the distance between the nearest RNA Pol II cluster to the *Sox2* locus in control condition without cohesin depletion.
(H) Plot of *Sox2* mRNA burst size vs. the distance between the nearest RNA Pol II cluster to the *Sox2* locus with cohesin depletion.
(I and J) Stack column of frequency of bursting events in proximal and distal cases in control condition (I) and cohesin depletion condition (J).
(K) Boxplot of condensate sizes (Mediator) in control condition (black box with all data points, n = 114) and cohesin depletion condition (red box with all data points, n = 76). Mean and standard deviation is 441 ± 173nm for the control condition and 411 ± 133nm for cohesin depleted condition.

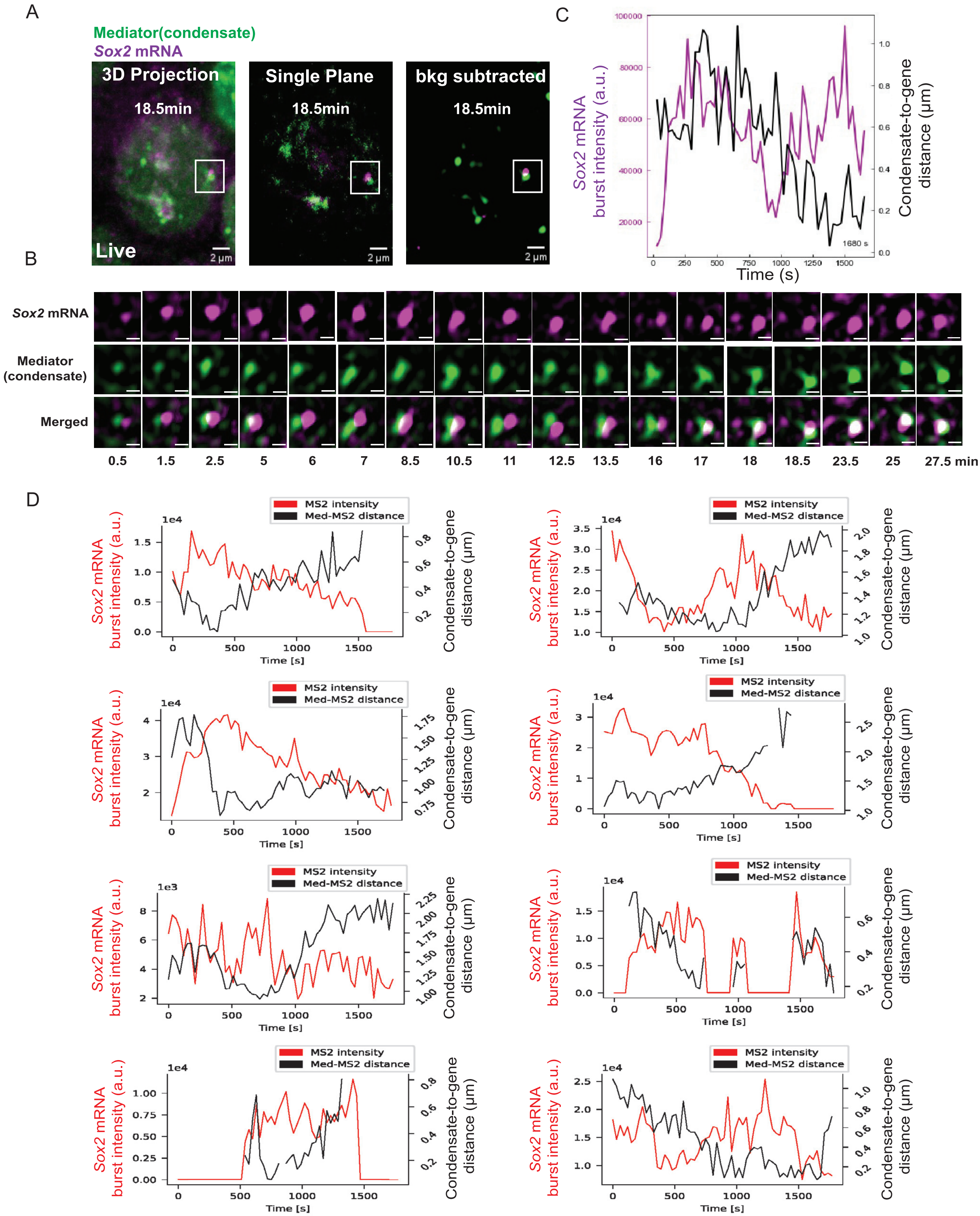

(legend on next page)

Figure S4. Condensate (Mediator) dynamically interact with the *Sox2* gene loci, related to Figures 3 and 4

(A) Left: maximum intensity z projection of a cell imaged using live-cell dual-color lattice light sheet showing colocalization of condensate (Mediator as a marker, labeled by Halo-JF_{646}, shown in green) with actively transcribing *Sox2* gene (shown in magenta) marked by MS2-tagged RNA (white box). Middle: single plane from the z stack. Right: maximum intensity projected image after background subtraction.

(B) Snapshot images of the condensate (Mediator) near the actively transcribing *Sox2* gene locus.

(C) Plot of *Sox2* mRNA burst intensity (left y axis) and the centroid-to-centroid distance of condensate-to-gene (right y axis) as a function of time. Scale bars, 2 μm.

(D) Example traces of *Sox2* mRNA burst intensity and condensate-to-gene distances. Data were taken in the three-color labeled cell line, and 8 example traces were shown. Real-time *Sox2* mRNA burst intensity is shown in red (left y axis), and real-time condensate-to-gene distance is shown in black (right y axis). Mediator is labeled as a marker of condensates.

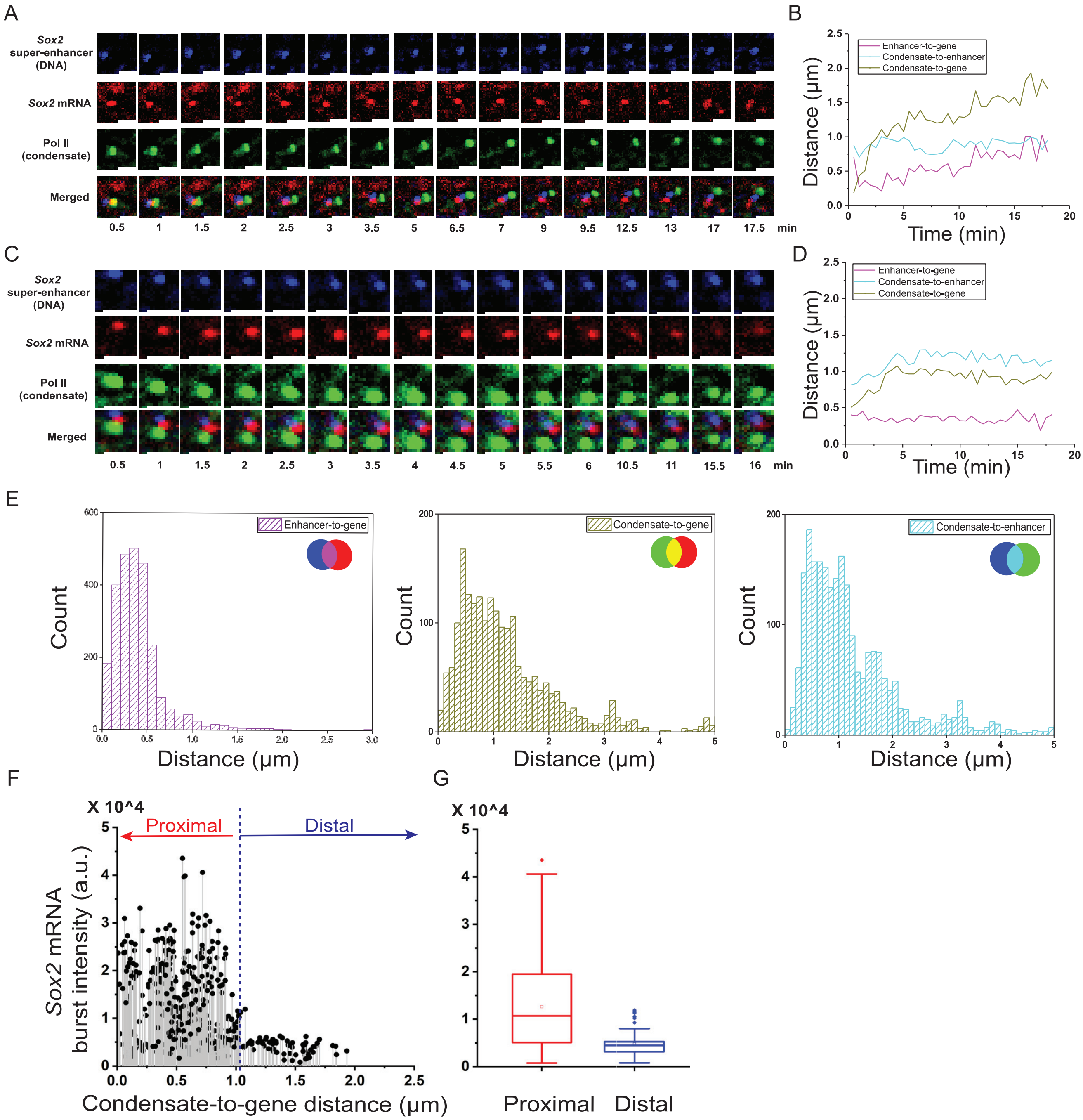

Figure S5. Condensate (RNA Pol II) dynamically interacts with both *Sox2* enhancer and gene while enhancer-to-gene distance stays relatively constant, related to Figure 4

(A and C) Snapshot images of three color labeled cell line in time lapse imaging. *Sox2* super-enhancer DNA (SCR) is labeled with CuO array shown in blue, *Sox2* nascent mRNA is labeled by MCP-SNAP (stained by JF_{646}) shown in red, and RNA Pol II condensates are labeled by JF_{549}-Halo shown in green.

(B and D) Quantification of centroid-to-centroid distances over time in the two cells. *Sox2* super-enhancer-to-gene distance is shown in magenta, condensate-to-gene distance is shown in yellow, and condensate-to-enhancer distance is shown in cyan. Enhancer-to-gene distance stays at ~300 nm and relatively constant, while condensate-to-enhancer and condensate-to-gene distances show a much larger variation, ranging from 200 nm to over 1 μm within 20 min of image acquisition.

(E) Histograms of centroid-to-centroid distances of enhancer-to-gene (shown in magenta), condensate-to-gene (shown in yellow), and condensate-to-enhancer (shown in cyan). The mean and standard deviations are 0.38 ± 0.27, 1.34 ± 1.11, and 1.37 ± 1.16 μm, respectively. Data were collected from time lapse traces of 31 cells.

(legend continued on next page)

(F) Plot of *Sox2* mRNA burst intensity vs. condensate-to-gene distance pooling all data points in each frame in the three-color cell line recapitulates the proximity-based enhancement. 494 total data points were collected from three-color lattice light sheet imaging of 15 cells.

(G) Boxplots of *Sox2* burst intensities in the presence of proximal RNA Pol II condensates (418 data points) and distal condensates (76 data points) using an arbitrary threshold of 1 μm. Black dots outside the whiskers are outliers representing the mostly enhanced burst intensities. Mean ± SEM is 12,632 ± 417 for proximal and 4,676 ± 251 for distal in arbitrary unit.

See also Video S3.

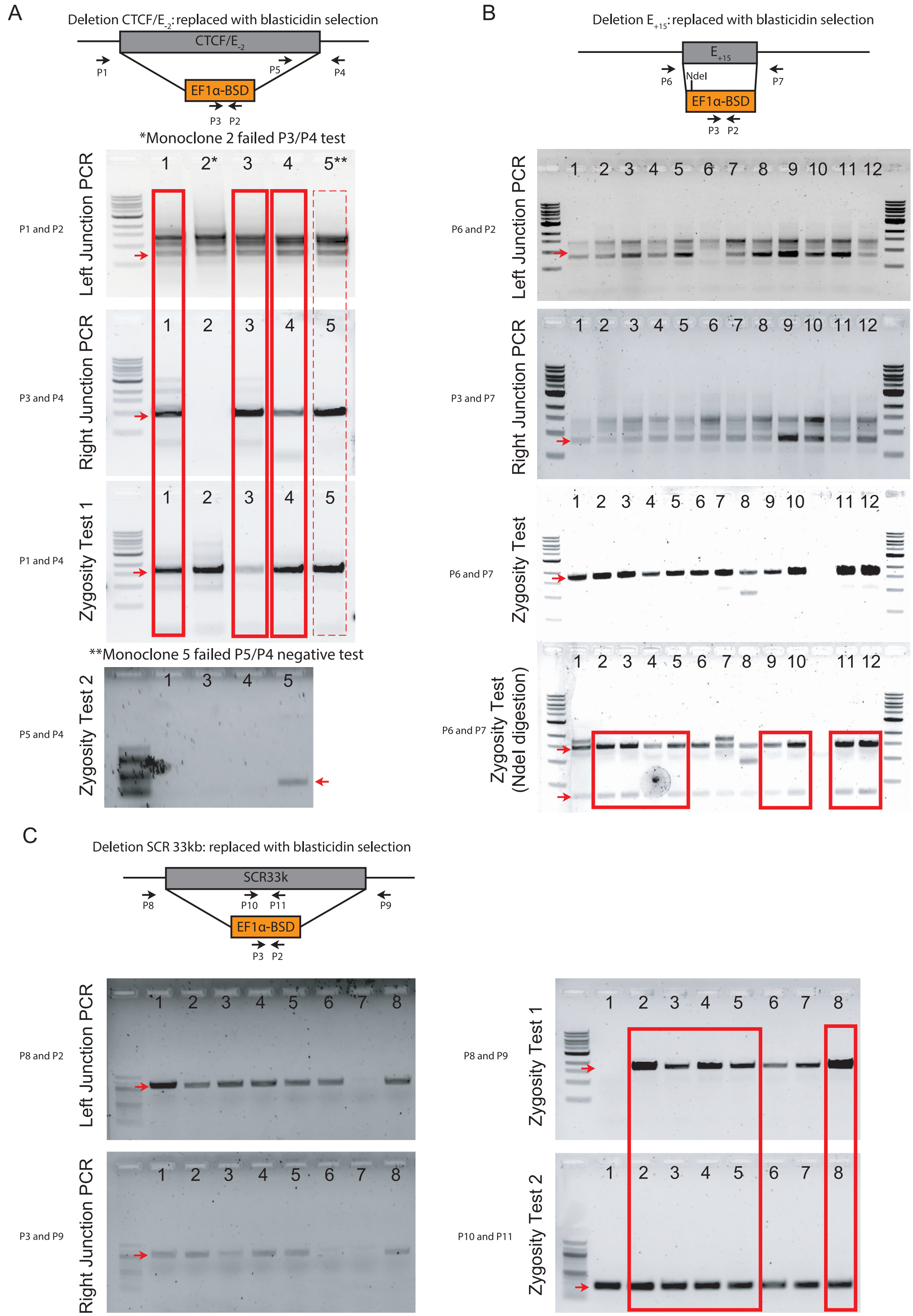

(legend on next page)

Figure S6. Confirmation of cell lines of CTCF/E_{-2}, E_{+15}, and SCR deletions by PCR and agarose gel assays, related to STAR Methods

(A) Schematic and gel assay results of CTCF/E_{-2} deletion monoclonals. gDNA from 5 monoclonals were extracted and PCR tested. Upper panel is schematic of CTCF/E_{-2} deletion, which is replaced by a blasticidin selection marker. P1 and P2 primers were used for left junction PCR, and expected band length is 879 bp. P3 and P4 primers were used for right junction PCR, and expected band length is 995 bp. To test zygosity, we used two sets of primers P1/P4 and P5/P4 for PCR. For homozygous deletion, we expect a band of 1.8 kb in P1/P4 PCR, and no band in P5/P4 PCR. Monoclonal 1, 3, and 4 have the right deletions and tested homozygous.

(B) Schematic and gel assay results of E_{+15} deletion monoclonals. gDNA from 12 monoclonals were extracted and PCR tested. P6/P2 were used for left junction PCR, and P3/P7 were used for right junction PCR. The expected band lengths are 827 and 854 bp respectively. To test zygosity, we first used primers P6/P7 for PCR. Since the deleted region is replaced with the blasticidin marker with a very similar length, we carried an additional NdeI digestion to differentiate from the non-deleted allele if it is heterozygous deletion. For homozygous deletion, we expect a band of 1.8 kb in P6/P7 PCR, and the purified 1.8 kb band should be digested into 1.5 kb and 300 bp without remaining 1.8 kb. If heterozygous deletion, there should be digested bands 1.5 kb and 300 bp, and also the remaining 1.8 kb. Monoclonal 2–5 and 9–12 have the right deletions and tested homozygous.

(C) Schematic and gel assay results of SCR deletion monoclonals. gDNA from 8 monoclonals were extracted and PCR tested. P8/P2 were used for left junction PCR, and P3/P9 were used for right junction PCR. The expected band lengths are 1,049 and 1,061 bp respectively. To test zygosity, we used two sets of primers P8/P9 and P10/P11 for PCR. For homozygous deletion, we expect a band of 1,853 bp in P8/P9 PCR, and no band in P10/P11 PCR. If it is heterozygous deletion, there is a band of 1,853 bp in P8/P9 PCR and also a band of 285 bp in P10/11 PCR. Monoclonal 2–5, and 8 has the right SCR deletion and are all heterozygous deletions. Red arrows in all panels indicate the expected band length. Red boxes indicate the monoclonals with the desired deletion.